

Maintaining a tubular discharge using a travelling electromagnetic wave results in a linear decrease in electron density along the plasma column from start to finish. This distribution of electron density corresponds to the power dissipated by the wave to heat the electrons in the discharge gas. The wave propagates in a vacuum along the outer wall of the dielectric tube, stopping when it runs out of power at a non-zero electron density value.

Michel Moisan

Groupe de physique des plasmas, Département de physique, Université de Montréal, Montréal H3C 3J7, Québec

Abstract

The experimentally recorded distribution of electron density along a plasma column supported by a travelling EM wave is linearly decreasing from start to finish; its slope depends strictly and solely on the gas pressure p , the frequency f of the wave and the internal radius R of the discharge tube. There are two opposing descriptive models: 1) an EM surface wave propagates along the three-constituent media of the tubular discharge, i.e., the plasma column, the dielectric tube and the outer wall of the latter. This model does not faithfully reproduce the linearity of the axial distribution of the electron density, at any rate always at the end of the column; 2) an EM wave propagates in a vacuum (ambient air) guided by the outer wall of the discharge tube, its electric field heating the electrons present in the gas and thus ionising it. As each electron thus obtained draws its energy from the E field of the wave, the axial distribution of the electron density can also be considered as a conservation relationship between the energy dissipated by the wave and the electron density produced. This model makes it possible in all circumstances to find a linear axial distribution of electron density from the beginning to the end of the column. The electron heating mechanism finally exhausts all the energy in the wave, so there is no more energy available for it to propagate otherwise, for example, along the dielectric tube or the plasma column. The origin of the linear behaviour of the electron density distribution lies in the stability condition of a discharge maintained by a travelling electromagnetic wave, which requires the electron density to decrease monotonically axially. This latter model is opposed to the model accepted by most theorists.

Keywords: Plasma physics, RF and microwave discharges, discharges sustained by electromagnetic surface waves/traveling waves.

+ This article is dedicated to the memory of Professor Ivan Zhelyazkov (1938-2021), plasma physics theorist (St. Clement of Ohrid University, Sofia, Bulgaria).

1. Introduction

Plasma columns sustained by the electromagnetic (EM) field of a travelling wave, incorrectly referred to until now as surface wave discharges (SWDs), have the advantage of being produced under an unequalled range of *operating conditions*. In the case of tubular discharges, these conditions are: the nature and density N of the gas (considered for gas pressures p typically of a few mTorr (a few Pa) up to twice atmospheric pressure), the internal radius R of the discharge (dielectric) tube (from 0.5 mm to 150 mm), and the frequencies f of the electromagnetic field, which range from radio frequency (RF) (as low as a few MHz) to microwaves (MW) (as high as 2.45 GHz). So-called SWDs have been extensively studied both experimentally (e.g. [1]) and theoretically (e.g. [2]) since the 1980s, leading to relevant new applications (e.g. [3]). The fact is that these are not SWDs but rather travelling wave discharges (TWDs), as will be shown. However, in our account of the published material, we will keep the name SWD in line with the chronology and change to TWD whenever possible given the level of explanation achieved.

The demonstration of the operation of a plasma column presented as supported by the propagation of an EM "surface" wave always attracts attention. In particular, the fact that the axial extension of the plasma column can be affected by closing the hand around the discharge tube has a spectacular effect.¹ Until now, it was accepted that the EM wave propagates along the plasma column and the dielectric tube, and that it depends on these media.

Our starting point for determining the nature and characteristics of this EM wave is the ascertainment that the axial distribution of electron density is experimentally linear along the length of the column, whatever the SWD operating conditions. The linearity of these axial distributions was objectively determined by a least-squares regression of the experimental data (Section 2). Six methods of diagnosing the electron density along the "SWD" plasma column were used (Appendix A). They all lead to a linear axial distribution of the electron density insofar as the diagnostic method takes into account all the electrons in the radial section at each axial position, which is not the case, for example, with the Thomson scattering diagnostic due to the narrowness of its laser probing beam. The fact that such complying data comes from five different research groups gives it even greater validity.

In section 3, the scientific literature leads us to the origin of the linearity of the axial distribution of the electron density in the case of travelling-wave sustained discharges: it derives from their stability condition ("steady state"), which requires the electron density to decrease monotonically along the axis (Sec. 3.1). The electric field component of the wave, through its relationship between the wave power attenuation coefficient $\alpha(z)$ and the electron density $\bar{n}_e(z)$, describes the heating of the electrons in the discharge gas and hence the ionisation of the plasma column (Sec. 3.2). The independence of the axial position of the product $\theta(z)S(z)$ (power per electron and cross-sectional area of the discharge tube) ensures the observed linearity of the axial distribution of the electron density up to the end of the plasma column (Sec. 3.3), a first in the field. In section 3.4, it is pointed out that from the final segment of the electron density axial distribution of the plasma column, however short it may be, our model allows us to trace back to a linear axial distribution of any length for given operating conditions. None of the previously published calculations have been able to show such a linear continuity of the electron density axial distribution, as the end of their column always shows some downward curvature of the electron density.

¹ This is hardly surprising since, as we shall see, the travelling wave that sustains the discharge propagates in the vacuum (ambient air) surrounding the discharge tube.

The properties identified in the previous paragraph and discussed below are used further on to analyse and comment on a selection of publications on "SWD" modelling in section 4. These papers can be divided into two categories: no specific property of the plasma column kinetics is introduced into the dispersion equation of the "surface wave" or, on the contrary, there is an assumed link between the wave and the plasma (coaction), Secs. 4.1 and 4.2, respectively.

In section 5, after the summary, the discussion focuses on points that are still obscure or missing, the resolution of which would help to provide a more complete understanding of the properties of plasmas maintained, as we shall have shown, by a travelling electromagnetic wave guided by the outer wall of the discharge tube. The conclusion highlights aspects that have previously been ignored or misinterpreted, and so far, grouped under the name of SWDs.

2. It is verified that beyond the antenna-like EM radiation region at the exit of the field applicator, the experimental distribution of the axial electron density of the travelling-wave (TW) plasma column is linear throughout and for all the values of the operating parameters p , f and R examined.

Foreword

In Glaude et al [4], the data points of the experimentally determined axial distributions of electron density along a TW-maintained plasma column were linearly related to each other to the best judgement of the operator, i.e. approximately. This was the case, for example, in figure 1a [5]. It was not until the early 2000s at the Université de Montréal (UdeM) that the experimental points were subjected to a linear least-squares regression (this type of software was not readily available before) to proceed with a recognised statistical method to ascertain the linearity of the axial electron density distribution. Using this statistical technique, figure 1b proves the validity of the previous approximate fit of the data points, meaning that the data points in our measurements naturally tend to align towards linearity, as confirmed by the (very) high coefficients of determination r^2 encountered. It should also be noted that the decreasing electron density does indeed stop abruptly at a non-zero value.

Believing that the straight line closest to the field applicator in figure 1a results from an TWD is a mistake because it ignores (as many have done) that this zone starting at the interstice of the field applicator is necessarily determined by its antenna-like behaviour (designated "space-wave radiation zone"), which generates an unguided (spreading in space with some lobes) and fast (speed of light) EM wave: this intrinsic radiation zone axially precedes any TW plasma column. The electron density axial distribution of this zone can take many shapes², its length depending on frequency as well as on the structural characteristics of the field applicator [6]. In [7], it was found that the axial extension of this radiation zone starting at the gap of a surfatron is between 0.13 and 0.4 of λ_0 (EM wavelength in free space), i.e., at 27 MHz between 1.4 m and 4.4 m. If we rely on the close-to-the launcher linear segment in figure 1b, the radiation zone would here extend on approximately 1.3 m long, which complies with [7].

² Figure 2a shows that the axial electron density distribution in the antenna-like region tends to become linear at low argon pressures (20-40 mTorr), whereas at higher pressures (80 mTorr and above) it appears bumpy.

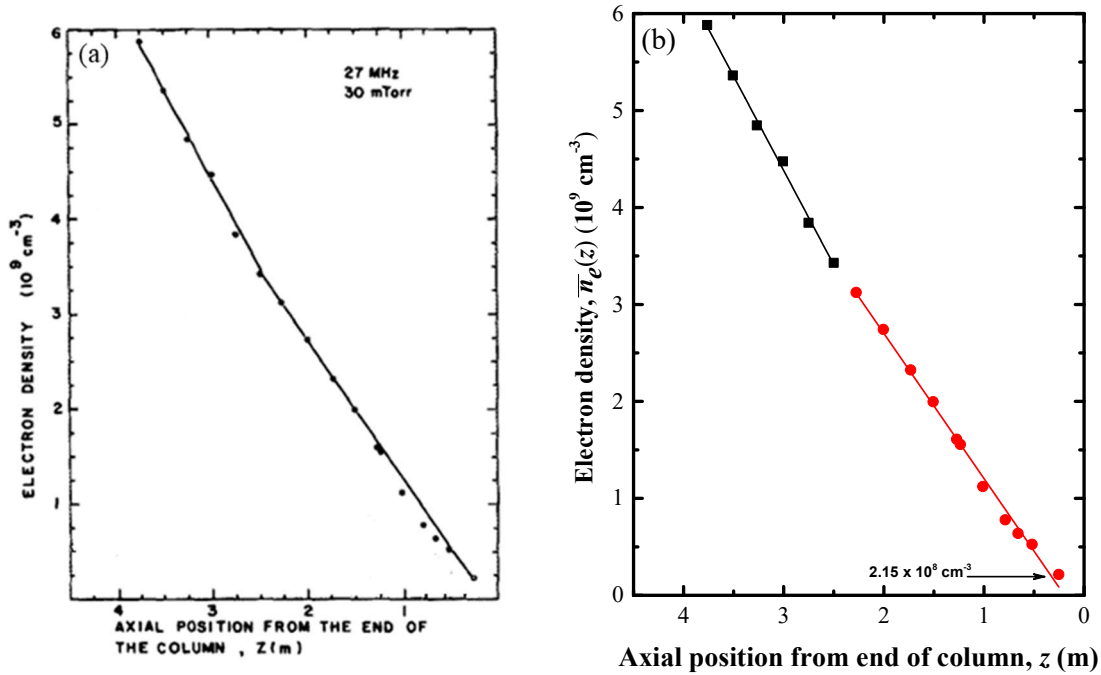


Figure 1: a) Electron density determined by the TW phase-variation method along the plasma column (Appendix A) at an argon pressure of 30 mTorr (7.5 Pa) in a discharge tube of 32 mm inner radius and at a wave frequency of 27 MHz. This curve was first published in 1985 as part of figure 3 in [5]: the data points were connected approximately to the eye by two successive straight lines; b) same data as in figure 1a), but processed by a least-squares regression, confirming the existence of two straight lines where $r^2 = 0.996$ for that of the antenna-like radiation zone and $r^2 = 0.994$ for the TWD. The observed electron density at the column end is about five times higher than the minimum electron density for TW propagation, namely $\bar{n}_{e(re)} = 4.8 \cdot 10^7 \text{ cm}^{-3}$ ((2) below): this is because even though the gas pressure is low enough to ensure a small collision frequency ν , ω is in this case too low to provide $\nu/\omega \ll 1$ (see Sec. 2.1 for details).

The linearity of the recorded axial distribution of SWD electron density is regularly questioned in the literature where least squares regression is not used, the axial distribution of electron density data often being described at best as "approximately linear"! All the corresponding experimental data presented in the present document have been subjected to a least-squares regression and found to be linear. Nevertheless, it cannot be asserted at this stage, based on statistical analysis (see Remark), that the axial distribution of TWDs is "purely" linear, which would reject the absence of possible small non-linearity.

Remark: The interpretation of experimental data for which r^2 is close to 1 as evidence of absolute linearity of the axial profile of the electron density is not justified: it only indicates a strong linear correlation. In fact, deviations above or below the mean value of the data points are masked when considering the quadratic value of the coefficient r .³ In practice, this means that a slight non-linearity in our data cannot be excluded at this stage even though the determination parameter r^2 is close to unity. A possibility is that the axial electron density distribution of TWDs be slightly non-linear, but this not being detectable unless the range of electron density considered is extended over 3 or 4 orders of magnitude: however, the largest observed range of electron density in a single

³ In fact, data points fitting a slightly curved distribution can give rise to a r^2 value close to unity: Figure 2 in [8].

measurement is less than two orders of magnitude for given discharge conditions, while spanning the range of the operating conditions enables to cover 16 orders of magnitude in electron density values ($2.2 \cdot 10^8$ - $4 \cdot 10^{14} \text{ cm}^{-3}$)!

The nature of the observed linearity in the axial distribution of the electron density is examined in all its possibilities and gradually clarified throughout this article, leading to a definitive physical conclusion: this distribution is perfectly linear and decreases axially, ending abruptly when the propagation of the travelling wave stops.

The axial gradient of electron density and its relationship with the operator-set conditions governing TWDs. As pointed out in the footnote ⁴, the discharge gas should be characterized by its density N (and its nature) instead of its pressure p . Up to now, the modelling effort on the axial gradient of electron density along SWDs have brought out into the open its dependence on the similarity-law factor ν/R , f and R being two genuine operating parameters (operator dependent only), while the electron-neutral collision frequency for momentum transfer ν is not since it can vary axially. We thus suggest appropriate to substitute N to ν (but it remains to be proven), yielding the following expression for the axial gradient of electron density:

$$\frac{d\bar{n}_e}{dz} = C_0 \frac{fN}{R} \quad (1)$$

where f , N and R are now all true discharge operating parameters, and C_0 is a constant. In fact, for practical reasons, the influence of discharge gas is most often expressed in terms of p instead of N .

2.1. Minimum electron density (end of plasma column) as a function of wave frequency and the role of the collisional parameter ν/ω exploring the whole TWD pressure range.

This section focuses on the minimum electron density necessary for the propagation of travelling waves whose stop marks the end of the plasma column. Throughout this section 2, it is experimentally verified that the minimum value of the electron density allowing the propagation of the travelling wave at a frequency f and in the low collision regime $\nu/\omega \ll 1$ in our configuration is obtained from the following relation [9]:

$$\bar{n}_{e(\text{re})}(\text{cm}^{-3}) \simeq 1.2 \times 10^4 (1 + \varepsilon_g) f^2 (\text{MHz}) \quad (2)$$

where ε_g is the relative dielectric permittivity of the discharge tube material (3.78 for fused silica and 4.52 for many brands of Pyrex glass). When ν/ω is no longer much less than unity, the minimum electron density is found to be higher than given by (2), the higher the gas pressure, the higher the electron density at the end of the column, a situation not always recognized as such [10], [11]. Note that although relation (2) was initially demonstrated for a SW sustained plasma [9], it accurately provides $\bar{n}_{e(\text{re})}$ in the case of the EM wave travelling in a vacuum outside the dielectric tube. As for the permittivity material, expected for SW propagation, this time it comes into play

⁴ The role and importance of the gas in a discharge is usually rendered by its pressure, p , an easily accessible and set quantity. A more appropriate parameter, however, is the gas density N . Indeed, p depends on the temperature T of the gas, since $N = p/k_B T$ (k_B is Boltzmann's constant), which indicates that p is not a distinctive physical parameter of the discharge since, for example, it can correspond to different N and T pairs. Another point, as mentioned, is that the value of N does not vary axially in the discharge tube, making it a condition fixed at the outset by the operator and not one whose value develops with plasma kinetics like the collision frequency ν [9].

by weakening the intensity of the wave's E field as it passes through the tube wall to heat the electrons in the discharge.

2.1.1. Low gas pressure case (0.02-0.3 Torr).

Figure 2a shows $\bar{n}_e(z)$, the radial averaged electron density, as a function of axial position from the end of the plasma column at five argon gas pressures (with almost doubling at the next). The electron density has been determined with a TM_{010} mode resonant-cavity method (Appendix A). It should be noted that it is only beyond a given axial position from the field applicator (a surfatron here [12]) does the axial distribution of the electron density becomes linear: the segment of the "curved line" of the electron density at higher axial positions than the straight line in the figure belongs to the antenna-like radiation region, which extends, as mentioned, for a distance of less than an EM vacuum wavelength from the output of the field applicator [7]. It is only beyond this position that a plasma column is generated by the guided (slow) wave which propagates in the vacuum surrounding the discharge tube and whose E field heats the electrons in the gas.

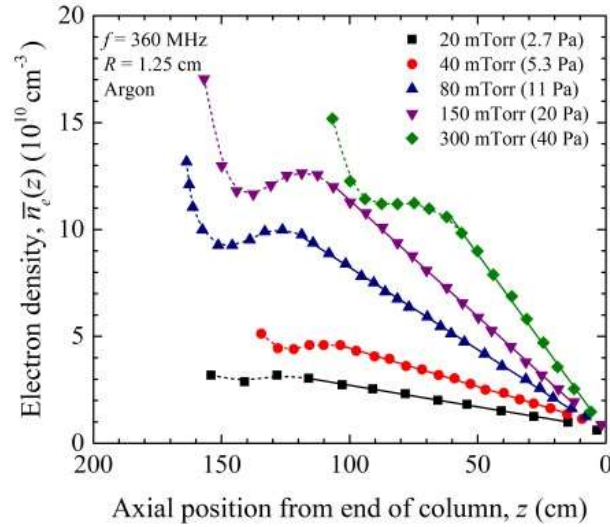


Figure 2a. Measured axial distribution of the radially averaged electron density, plotted from the end of the plasma column, along the discharge sustained by the propagation of a TW at 360 MHz, at five argon gas pressures in a Pyrex-brand glass (Dow Corning: 4.52 relative permittivity) discharge tube of internal radius 12.5 mm and external radius 15 mm [4].

Figure 2b corresponds to the 0-50 cm axial part of figure 2a. These curves were plotted from linear least-squares regressions on (many) data points, yielding coefficients of determination r^2 very close to unity (see caption for their values) for gas pressures between 20 and 300 mTorr; the slope of the axial electron density distribution steepens with increasing pressure, as predicted by relationship (1) if we consider N to be proportional to gas pressure p . The observed axial distributions of electron density are clearly straight lines that extend as such to the end of the plasma column.

Figure 2b also shows that the minimum electron density $\bar{n}_{e(re)}$ (2) for wave propagation is reached at 20 mTorr for 360 MHz; this is clear proof that the travelling wave supporting the plasma column obeys (2) at its very end. In [4] under current operating conditions, ν is calculated to be about $1 \cdot 10^8 \text{ rad s}^{-1}$, which at 360 MHz gives ν/ω about 0.04, verifying $\nu/\omega \ll 1$.

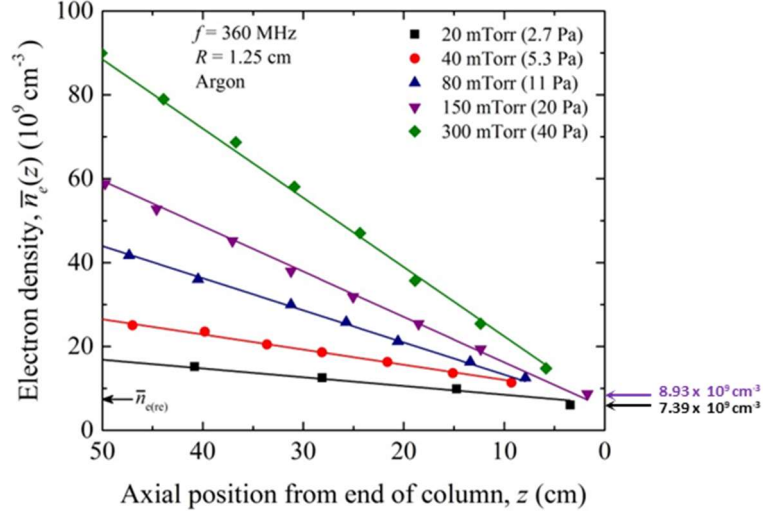


Figure 2b. Enlargement of the axial segment 0-50 cm in figure 2a. The experimental data points for a given gas pressure all fit a straight line to the very end of the plasma column, with $r^2 = 0.984, 0.995, 0.995, 0.999,$ and 0.999 at 20, 40, 80, 150, and 300 mTorr, respectively. The corresponding minimum theoretical electron density assuming no collisions (2) is $\bar{n}_{e(\text{re})} = 7.4 \cdot 10^9 \text{ cm}^{-3}$ as indicated by the arrow inside the figure frame. The minimum measured electron density values at 20 and 40 mTorr are indicated by the corresponding arrow on the outside of the figure, indicating that the $\bar{n}_{e(\text{re})}$ is reached here at 20 mTorr.

2.1.2. Intermediate pressure range case (0.12-7.2 Torr). This case corresponds, given the gas pressure and TW frequency, to the collisional regime varying from $\nu/\omega \ll 1$ to $\frac{\nu}{\omega} < 1$. Knowing that according to relationship (1), the axial gradient of electron density $\frac{d\bar{n}_e}{dz}$ depends on the radius of the discharge tube in $1/R$, this means that the ratio of the slope of the electron axial density in figure 3a to that in figure 3b should be $R_b/R_a = 1.7$, whereas the ratio of the measured slope values, $6.35/4.77 = 1.33$, is lower. One possible explanation is that there is some radial contraction of the plasma column (the plasma does not fill the discharge tube radially) in the tube with the larger radius, so that the radius of the plasma column corresponding to it is smaller (on average axially) than R_b . The axial profile of the electron density $\bar{n}_e(z)$ is obtained here by determining the phase variation of the travelling EM wave along the plasma column, then calculating the electron density using the wave phase diagram (Appendix A).

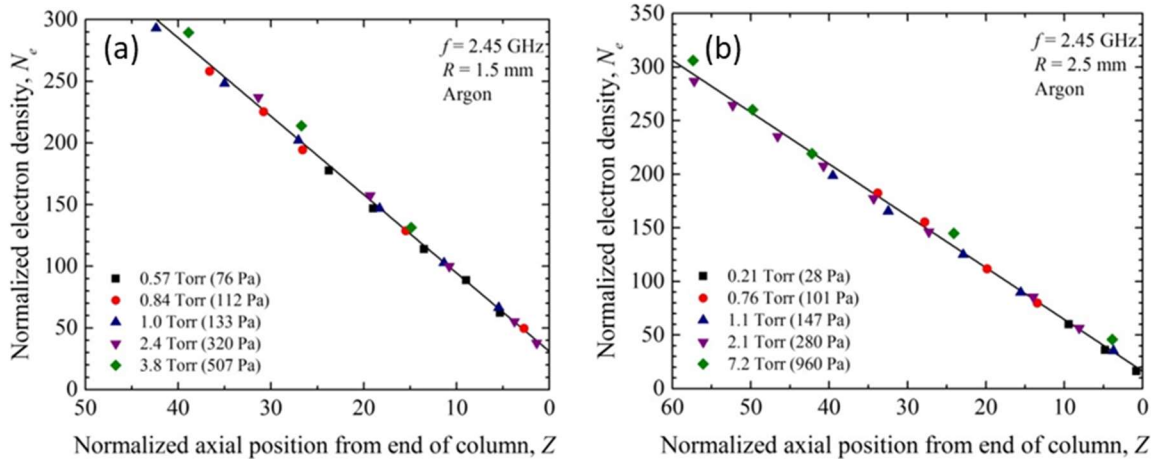


Figure 3 (foreign laboratory). Axial distribution of electron density of a TWD sustained at 2450 MHz at argon gas pressures in the low to some medium collisional regime in two sets of discharge tubes ($\epsilon_g = 4.8$): a) $R = 1.5$ mm with $r^2 = 0.995$ and b) $R = 2.5$ mm with $r^2 = 0.995$. The figures are adapted from [13] where the normalized electron density N and axial position Z are defined and the coefficient of determination r^2 have been added.

2.1.3. Atmospheric pressure domain. Figure 4 illustrates the observed axial distribution of the radially averaged electron density along a TW-supported plasma column at twice atmospheric pressure in argon gas [14]. The electron density is determined from the broadening of the H_β line (486.1 nm) (Appendix A) with an argon-hydrogen gas mixture containing 0.5 % hydrogen.

Although v/ω is much larger than unity this time, unlike in section 2.1.2, the data still follow a straight line (except for the point $z = 20$ cm for $R = 0.97$ mm, which belongs to the radiation region of the field applicator (surfatron)). The smaller the value of R , the steeper the corresponding slope of the axial electron density distribution, as predicted by relationship (1). It should be noted that the internal radius of these three tubes is small enough (less than one mm) to ensure that they are filled by the argon discharge (no radial contraction of the plasma). Another feature worth highlighting is that these discharge tubes are thick-walled (all with an external radius of 8 mm), whereas all the other tubes appearing in this report are comparatively thin-walled (e.g., $R = 12.5$ -13 mm for an external radius of 15 mm in figure 2).

For the reasons given in paragraph 2.1, the value of the electron density at the end of the column in high-pressure gas discharges should exceed the minimum electron density (2) for TW propagation, which at 915 MHz and with $\epsilon_g = 3.78$ is $\bar{n}_{e(\text{re})} = 4.8 \cdot 10^{10} \text{ cm}^{-3}$, whereas the electron density measured at the end of the column in the figure is $2 \cdot 10^{14} \text{ cm}^{-3}$ in the 0.97 mm radius tube and higher in the smaller tubes, meaning four orders of magnitude higher as envisaged!

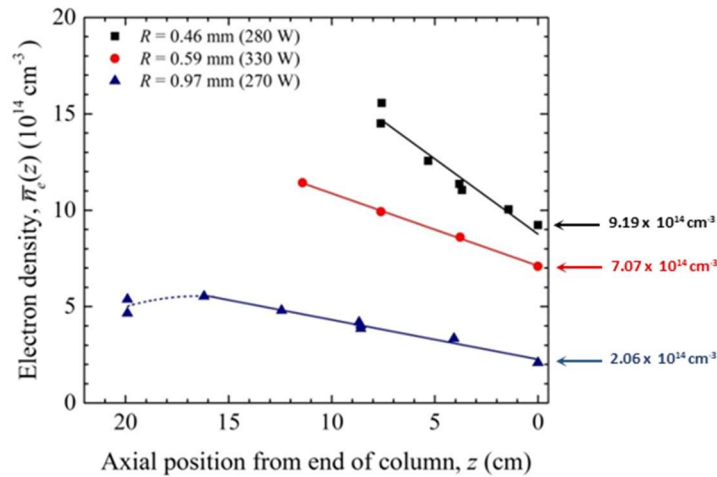


Figure 4. Measured axial distribution of radially averaged electron density displayed from the end of the plasma column supported by a 915 MHz TW in fused silica discharge tubes of three different internal radii (all thick-walled tubes of 8 mm external radius), in argon gas at twice atmospheric pressure (after [14]). Electron density measurement made through H_β Stark broadening (Appendix A). Determination coefficient $r^2 = 0.935, 0.999, 0.977$ following the increase of the tube radius. Here $\bar{n}_{e(\text{re})} = 4.8 \cdot 10^{10} \text{ cm}^{-3}$ is four orders of magnitude lower than the measured electron density.

The pressure range we have just examined extends from a few mTorr up to twice atmospheric pressure, which implies major changes occurring in the recombination mechanism of the plasma charged particles, moving from the diffusion regime (free then ambipolar) to volume recombination (atomic and molecular). The kinetics of the discharge are therefore strongly

modified by the passage through these different regimes. However, the linearity of the axial distribution of the electron density is not affected over this very wide pressure range.

According to *Kovačević et al. (Sec. 4.2.5)*, based on SWD calculations, the linearity of the axial electron density distribution is lost with thick-walled dielectric tubes if a SW is assumed to propagate along them due to increased dielectric losses owing to tube thickness and high EM wave frequencies [15]. Figure 4 in this section shows that this is not the case, since linearity is preserved, for example, with a tube having an outer/inner radius ratio of 8 mm/0.46 mm. The reason for this is that there is no propagation of the TW along the dielectric tube, but only in the vacuum surrounding the outside of the discharge tube.

2.2. Axial distribution of recorded electron density as a function of the travelling wave frequency

Figures 2 at 360 MHz, 3 at 2450 MHz and 4 at 915 MHz have already shown, among other things, that experimentally varying the surface wave frequency does not affect the linearity of the TWD axial electron density distribution. The coming section looks in more detail at the influence of the wave frequency range on the slope of the axial electron density distribution.

2.2.1 Covering part of the RF domain up to the beginning of the microwave domain (27-200 MHz). Figure 5 shows the axial distribution of the measured radially averaged electron density (using the TM_{010} resonant cavity method) referenced from the end of the plasma column, $\bar{n}_e(z)$, at four frequencies of the travelling wave ranging from the RF domain (27 and 50 MHz) to the beginning of the microwave range (100-200 MHz) [16]. To each of these frequencies corresponds a linearly decreasing axial electron density distribution with a very high coefficient of determination r^2 of least-squares regression (see the figure caption). The slope of these lines increases with the TW frequency, according to relationship (1).

A correlative result of the linearity of the axial distribution of the TWD's electron density, noted from the very beginning of SWD studies, is the fact that increasing the EM power transmitted to the field applicator, under given operating conditions, results in an increase in the length of the plasma column without altering the slope of the axial distribution of its electron density. The best way to see this is to plot the electron density axial distribution in relation to the end of the plasma column. The 100 MHz curve in figure 5 illustrates this very well: the arrow pointing towards 36 W represents the axial position of the beginning of the TW plasma column relative to its end at this power value and, as we have just seen, the slope of the already existing segment of the plasma column is not altered when the MW power is increased to 58 W.

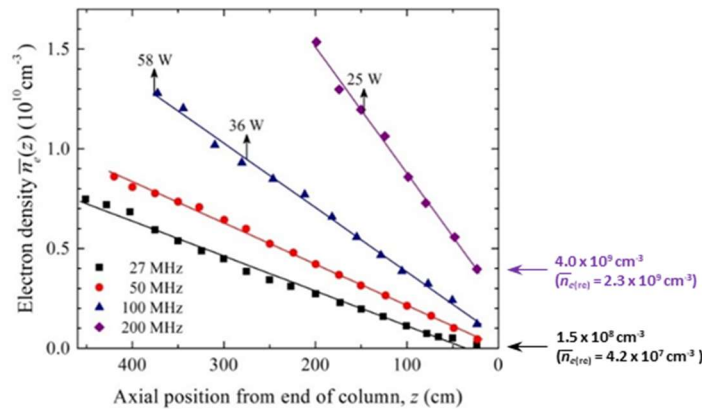


Figure 5. Radial mean value of the measured electron density, using the TM_{010} resonant cavity method, as a function of axial position along the plasma column from its end. The discharge is obtained by propagating an EM travelling wave excited at four different frequencies, in argon gas at a pressure of 30 mTorr (4 Pa)

and in a fused silica tube of 32 mm internal radius [16]. The lines drawn result from least squares regressions on the data, providing coefficients of determination $r^2 = 0.990, 0.999, 0.998, 0.998$ with increasing frequency.

2.2.2 Covering the 200-2450 MHz MW range. Figure 6 shows the measured axial distribution of the radially averaged electron density at 210 and 2450 MHz, at a gas pressure of 200 mTorr (27 Pa). The least-squares linear regressions give at 210 MHz, $r^2 = 0.991$ for the antenna-like segment and $r^2 = 0.984$ (4 points only) for the travelling wave-sustained one while at 2450 MHz with $r^2 = 0.997$ there is no sign of an antenna-like zone as expected [7]. However, according to (1) the slope of the distribution at 2450 MHz should be steeper than that at 210 MHz. This discrepancy is attributed to the fact that the TW plasma column is partially radially contracted in the $R = 4.5$ mm tube at 2450 MHz, whereas it is not at 210 MHz (see 2.3.3 below).⁵ As for the measured minimum electron density (the value at the end of the column), as indicated with an arrow in the figure it is 3.23 and $8.67 \times 10^{11} \text{ cm}^{-3}$ at 210 MHz and 2450 MHz, respectively, while the minimum electron density calculated from (2) (assuming $v/\omega \ll 1$ and with $\epsilon_g = 4.52$) is 2.9×10^9 and $3.9 \times 10^{11} \text{ cm}^{-3}$, respectively. The electron density at the end of the column is closer to $\bar{n}_{e(\text{re})}$ at 2450 MHz than at 210 MHz, due to a lower v/ω ratio, apparently well below unity if the near equality of measured and theoretical electron density values is anything to go by.

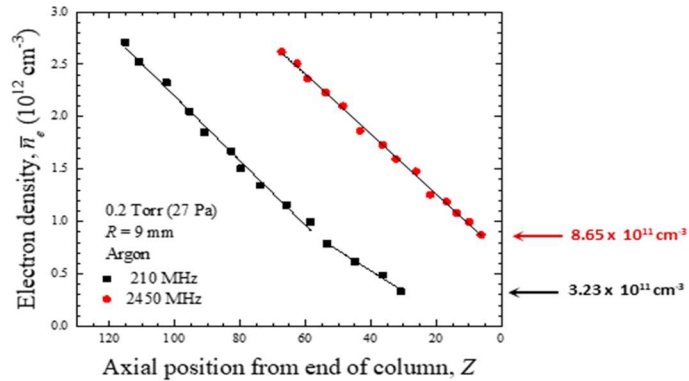


Figure 6. Measured axial distribution of the electron density (using the TM_{010} resonant cavity method) of a TWD held in argon at 27 Pa in a fused silica discharge tube with an internal radius $R = 4.5$ mm at 210 and 2450 MHz. Least-squares linear regression gives at 210 MHz, $r^2 = 0.991$ for the antenna-like segment and $r^2 = 0.984$ (4 points) for the travelling wave-sustained one while at 2450 MHz there is no sign of an antenna-like zone as expected, with $r^2 = 0.997$ (adapted from [16]). The calculated cut-off electron density for TW propagation at 210 MHz and 2450 MHz assuming $v/\omega \ll 1$ is $\bar{n}_{e(\text{re})} = 2.9 \times 10^9 \text{ cm}^{-3}$ and $3.9 \times 10^{11} \text{ cm}^{-3}$, respectively.

Figures 5 and 6 showed that the linearity of the electron density axial distribution is maintained over the entire 27-2450 MHz range. As mentioned, the range of operating conditions covers 16 orders of magnitude in electron density values (2.2×10^8 - $4.10^{14} \text{ cm}^{-3}$)! Such a large variation in electron density should ultimately affect the electron energy distribution function (EEDF): the EEDF is certainly not Maxwellian in the low electron density plasma of 27 MHz, but its shape should gradually tend towards a Maxwellian one as the electron density increases with the TW frequency approaching 2450 MHz. Nevertheless, it is observed that even such large variations of electron density and of the v/ω ratio with the TW frequency do not affect the linearity of the axial

⁵ The slope of the axial distribution of the electron density of a given TW discharge (p, f and R) is found experimentally to decrease as the plasma contracts.

electron density distribution, leading to the conclusion that the TW behavior does not depend on any EEDF characteristics.

Figure 7 shows the axial distribution of the radial mean electron density measured in a tube of the same radius at both 915 and 2450 MHz, at atmospheric pressure, this time in neon gas. The behavior of the corresponding axial distribution of the electron density, obtained by a least squares regression on the collected data, is again linear but with a lower r^2 value than those quoted above due to a smaller number of experimental points (only 4 and 5 data points at 915 and 2450 MHz, respectively). The slope at 2450 MHz is actually steeper than at 915 MHz in agreement with relation (1), having in mind that at the same time that radial contraction is less likely to occur in neon than in argon for a given R [17].

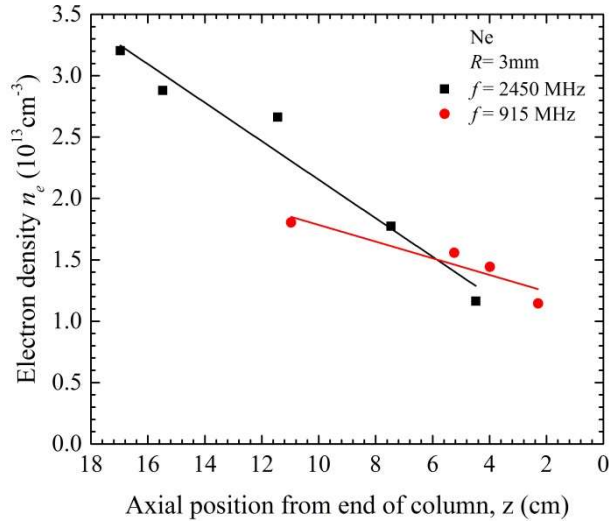


Figure 7. Measured axial distribution of radially averaged electron density, displayed from the end of the plasma columns sustained by a TW at 915 MHz and 2450 MHz in a fused silica discharge tube with 3 mm inner radius, in neon gas at atmospheric pressure [18]. Electron density was determined from the broadening of the $H\beta$ line (486.1 nm), hydrogen atoms supplied by a minimal amount of water vapor in the discharge gas. Coefficients of determination of the least-squares regression $r^2=0.80$ and 0.95 for 915 and 2450 MHz, respectively, noting that assigning r^2 values to few and rather scattered experimental data points is debatable.

2.3. Axial distribution of electron density recorded in tubes with different internal radii under low and high collision regime

2.3.1. Low-collisional regime. Figure 8 shows the measured axial variation of the mean radial electron density along the plasma column supported by a 100 MHz TW, for two values of the inner radius R of the fused silica discharge tube, in argon gas at a pressure of 1.8 Pa (10 mTorr) [16]. Again, the experimental electron density points, after a least squares regression, give a straight line for each value of R . When decreasing R , the corresponding slope becomes steeper, as shown in the figure, in accordance with the relationship (1).

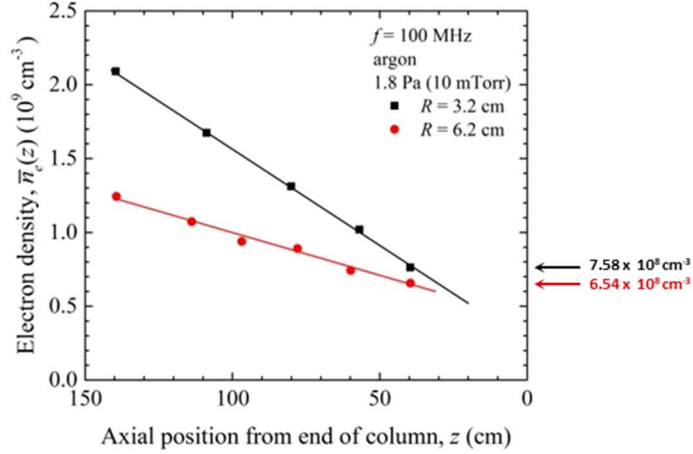


Figure 8. Measured axial distribution of the mean radial value of the electron density with respect to the end of the plasma column supported by a 100 MHz TW for two values of the internal radius R of the discharge tube, in argon gas at the very low pressure of 1.8 Pa (10 mTorr) [16]. The electron density in the $R = 32$ mm was determined using a TM_{010} resonant cavity method, while the axial phase variation of the TW was used for the larger $R = 62$ mm tube. [19]. The coefficients of determination of the least-squares regression are $r^2 = 0.993$ and 0.986 for $R = 32$ mm and 62 mm, respectively. The calculated electron density at the end of the TWD plasma column at 100 MHz assuming $\nu/\omega \ll 1$ is $\bar{n}_{e(\text{re})} = 6.62 \cdot 10^8 \text{ cm}^{-3}$, which corresponds, within the experimental error, to the value measured in the tube of larger radius.

2.3.2. High-collisional regime. Figure 4 above already showed the measured axial distribution of radially averaged electron density in a TWD supported at 915 MHz in argon gas at atmospheric pressure, which specifically concerned discharge tubes of three different inner radii. The r^2 value of their axial electron density distribution confirmed their linearity. At the same time, this indicates that even at atmospheric pressure, the smaller the value of R , the steeper the corresponding slope of the axial electron density distribution, in agreement with relationship (1).

2.3.3. The radial contraction of the plasma column is responsible for an axially inhomogeneous plasma, which nonetheless does not affect the linearity of the axial electron density distribution. In the low collision regime, the TW plasma generally fills the discharge tube radially. However, at pressures approaching one Torr or more, radial plasma contraction does occur if the value of one or more of the following parameters reaches a certain relative magnitude: the radius of the discharge tube, the frequency of the wave and the pressure of the discharge gas and its mass [17]. In the case of figure 9, operation at atmospheric pressure is decisive in achieving plasma contraction, helped by a relatively large tube radius and a wave frequency in the upper range of microwaves; however, the lower mass of neon compared with argon is less favourable to this effect. Radial contraction, as shown in figure 9, means that the radius of the plasma column decreases continuously towards its end.



Figure 9. Photograph of a 915 MHz contracted neon TWD at atmospheric pressure (inner radius of the discharge tube 6 mm) showing that the radius of the plasma column decreases continuously towards its end, making it structurally inhomogeneous in the axial direction (after [17]).

In the case of an already contracted TWD plasma column, increasing the inner radius of the tube causes the plasma column, at a given axial position, to move further and further radially away from the discharge tube wall [17], [18]. At the same time, the slope of its axial electron density distribution becomes gentler. In contrast, when the inner radius of the tube is small enough to show no sign of radial contraction of the plasma column, the slope of the axial electron density distribution, as expected from (1), becomes steeper when its radius is reduced. The degree of contraction observed at atmospheric pressure depends strongly on the mass of the gas: for example, at 2450 MHz, it is clearly marked in a tube of $R = 3$ mm with argon, even more so in krypton but absent in helium⁶.

A radially contracted plasma column, as illustrated in the figure, is structurally an axially inhomogeneous medium. Nevertheless, its axial distribution of electron density remains linear, as in the case of an uncontracted plasma column. This is because the surface wave dispensing power to the plasma does not propagate on it, but only in the vacuum embedding the discharge tube, as we will conclude analytically from section 3 further on.

2.4. Axial distribution of electron density observed under different gas flows

It is interesting to check to what extent the variation in the gas flow rate in the discharge affects the axial distribution of the electron density of the plasma column driven by a travelling wave. Since the gas density N is constant in a discharge tube of constant cross-section, this should not affect the linearity of the axial distribution of the electron density in accordance with relationship (1). On the other hand, increasing the flow velocity of a gas in a tube decreases its (inlet) pressure (Bernoulli's law), and therefore possibly the value of N and, by (1), its slope, as is the case.

The experiment was carried out in argon at atmospheric pressure in a (fused silica) tube with a sufficiently small internal radius (0.75 mm) to avoid radial contraction of the plasma and possible filamentation, at gas flow rates of 0.25 and 1 standard litre per minute (slm) in an open-ended tube. The discharge is performed at 2450 MHz using a surfaguide, an E -field applicator with a launching gap on each side of the waveguide structure, producing two plasma columns which, depending on the direction of the gas flow, are described as forward and backward. These two columns a priori receive an equal share of the power emitted by the surfaguide, but the columns in the opposite direction to the gas flow are shorter as shown in figure 10. The electron density is obtained by broadening of the H_β Balmer line (486.1 nm). The key point to note from this figure is that the axial distributions of electron density remain linear in all cases and that the slope corresponding to the greatest gas flow rate (smallest value of N) is the smallest, both forwards and backwards, which is consistent with the role of N in relation (1).

⁶ The higher the mass of the noble gas, the smaller the tube radius needs to be for the plasma to fill it radially. For example, an argon TW discharge undergoes contraction in a tube with a radius of just a few mm, but this requires tubes with a much larger radius in helium gas [20].

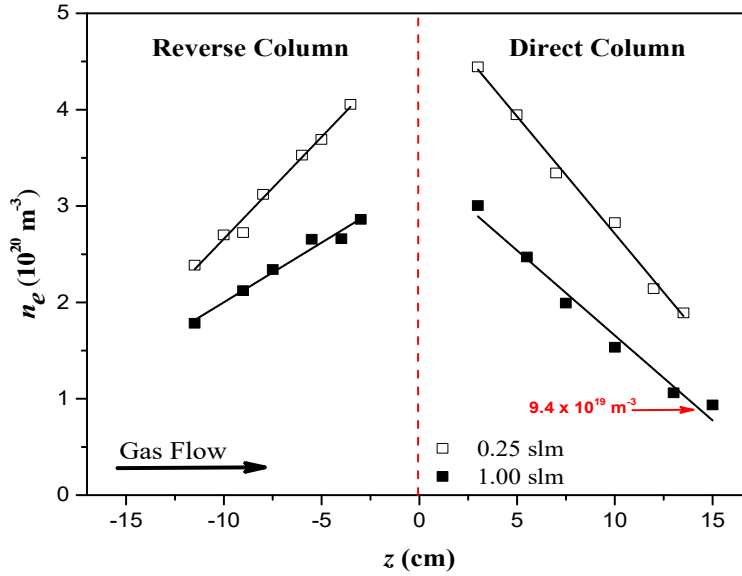


Figure 10 (foreign laboratory). Measured axial distribution of the plasma column electron density according to argon gas flow direction (forward and backward) for two gas flow rates at atmospheric pressure. The electron density is determined by broadening of the H_{β} Balmer line (486.1 nm). The data points from [21] were processed by least-squares regression yielding for the 0.25 slm reverse and direct column $r^2 = 0.985$ and 0.992 , respectively and for the 1 slm reverse and direct column $r^2 = 0.971$ and 0.974 , respectively. Since the theoretical minimum electron density for TW propagation $\bar{n}_{e(\text{re})}$ (2) here is $1.7 \cdot 10^{16} \text{ m}^{-3}$, the TW is therefore observed to cease propagating at more than three orders of magnitude in electron density from $\bar{n}_{e(\text{re})}$, according to the mechanisms described in Sec. 2.1.

2.5. The case of molecular gases

The figures above showed TW discharges in noble gases (argon, neon), in fact essentially composed of atoms. In contrast, molecular gas discharges at low electron densities are mainly made up of molecular ions, whereas at high electron densities they involve more and more atomic ions due to a higher rate of molecular dissociation. Difference in concentration between atoms and molecules in these discharges will be shown to have no effect on the linearity of their axial electron density.

2.5.1. Nitrogen. Figure 11 depicts a TWD of N_2 maintained at 500 MHz, in a Pyrex™ glass tube ($\epsilon_g = 4.52$) with an internal radius of 22.5 mm and a gas pressure of 0.5 Torr [22]: this case represents a medium-frequency TWD, in a tube with a relatively large radius but with a gas pressure of less than one Torr, conditions corresponding here to an uncontracted discharge. The electron density has been determined with the Langmuir probe technique (Appendix A). Here, $\bar{n}_{e(\text{re})}(\text{cm}^{-3}) = 1.66 \cdot 10^{10} \text{ cm}^{-3}$ (indicated by the arrow on the frame of the figure), a value well above the minimum electron density measured by the authors. Reporting an electron density well below the minimum value for TW propagation means that the Langmuir probe diagnosis in this case is inappropriate as it contradicts the demonstration provided by the TM_{010} resonant cavity (Figure 2b) and the TW axial phase variation (Figure 8) of the minimum electron density $\bar{n}_{e(\text{re})}$ for TW propagation (section 2.6.3).

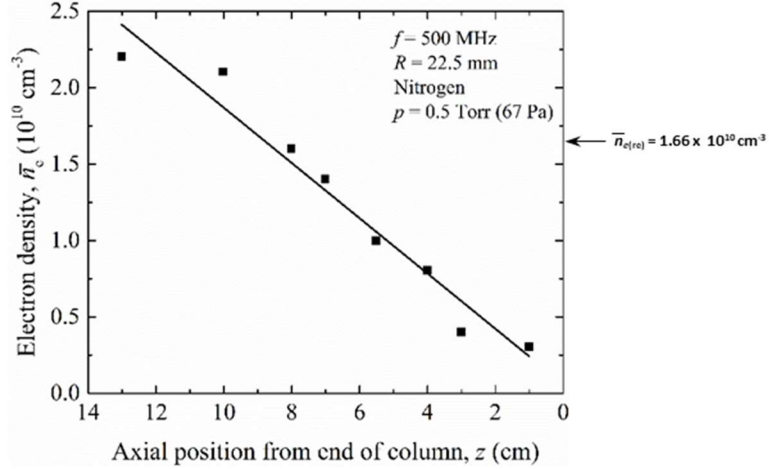


Figure 11 (foreign laboratory). Axial electron density distribution determined with a Langmuir probe technique for a TWD sustained in N_2 gas at 67 Pa in a discharge tube ($\epsilon_g = 4.52$) with inner radius $R = 22.5$ mm at 500 MHz. Least-squares regression of the data points gives a linear fit with $r^2 = 0.986$ (adapted from [22]).

2.5.2. Hydrogen. Figure 12 reports the measured axial distribution of electron density in an H_2 TWD [23] again using a Langmuir probe. The data point $Z = 28$ (normalized axial position) is assigned to the radiation region of the field applicator antenna [7] and is therefore not part of the TW plasma column. As in the previous section, the results of diagnosing electron density using a Langmuir probe are incorrect in the current situation, as we will see in more detail in section 2.6.3.

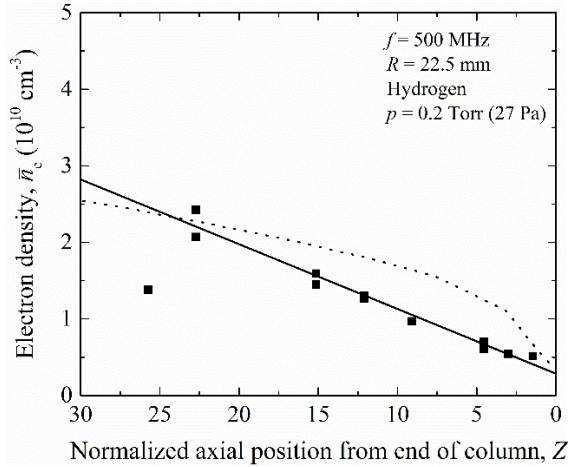


Figure 12 (foreign laboratory). Measured axial distribution of the electron density of a TWD held at 500 MHz in H_2 gas at 27 Pa in a PyrexTM glass discharge tube ($\epsilon_g = 4.52$) with an internal radius of 22.5 mm [23]. Langmuir probe diagnostic was used for determining electron density. The least-squares regression, excluding the value at the largest Z (related to the antenna-like region of the field applicator), gives $r^2 = 0.948$. The dotted curve is theoretical, adapted from [23], and will be recalled in Sec. 4.2.6: it clearly deviates from experiment.

2.6. In the case where there is radial contraction of the TWDs, measurement of their electron density along the plasma column leads to a linearly decreasing axial electron density distribution only provided the total number of electrons in each radial section along the plasma column is taken into account.

2.6.1. The total number of electrons in a radial section of the plasma column at a given axial position is proportional to the power dissipated there by the travelling wave. Recalling the concept of power absorbed per electron [9], it is easy to imagine that the total number of electrons created in a radial section of the plasma column is proportional to the power absorbed from the wave to generate them at this axial position.

Electron density diagnosis with the TM_{010} resonant cavity takes this total number of electrons into account, since the entire radial distribution of electrons is exposed to the electromagnetic field present in the cavity. In a different way, but with a similar result, the axial variation of the TW phase provides an average value of the total number of electrons over the entire radial section of the plasma column at each axial position. In both cases, the graph of the radially averaged electron density is therefore proportional to the power lost by the wave at that axial position: this is an additional and innovative way of looking at the axial distribution of the electron density, which then appears as expressing a law of conservation of energy linking the wave and the electrons of the plasma column (as first proposed by Aliev et al. [26]). The case where the electron density diagnosis considers only part of the radial distribution takes a particular turn when the plasma column is subjected to radial contraction, as we will see in the next section.

The fundamental reason why the power dissipated by the propagating wave decreases linearly with axial position is determined, as we shall see later (Sec. 3.1), by the condition ensuring the stability of the discharge under stationary state. This condition requires the wave that heats the electrons in the gas column (and ionises it) to be a travelling wave, without the need to specify its properties further. The link between the power dissipated axially by the wave and the corresponding electron density is direct and unique. As shown below, $\alpha(z) = \frac{b}{\bar{n}_e(z)}$ (21) where $\alpha(z)$ is the attenuation coefficient of the wave and b is axially constant. There is no other connection between the travelling wave and other specific properties of the plasma column.

2.6.2. The case of electron density diagnostics where all electrons in the radial distribution are not accounted for. Let's first consider the instance where there is no radial contraction of the plasma column: under these conditions, the radial structure of the plasma column does not vary axially, so that whatever section of the radial distribution of electrons is taken into account (which depends on the diagnostic technique used), it always remains axially proportional to the total number of electrons in the radial distribution, and therefore to the power dissipated along the axis by the surface wave, leading to a linear distribution of the electron density of the plasma column. This is what happens in figure 6 at 2450 MHz for $R = 4.5$ mm, where there is radial contraction of the plasma column, but the measured axial distribution of the electron density remains linear because the TM_{010} diagnostic method considers the total number of the electrons in the radial distribution.

The situation is different when there is radial contraction of the plasma since the radius of the plasma column decreases axially towards its end (figure 9). Under these conditions, it is only when taking into account the total number of electrons in their radial distribution that proportionality with the power dissipated axially by the wave is preserved as a function of axial position. This proportionality is indeed lost when only part of the radial distribution of electrons is considered in diagnosing the electron density, as is the case with the Thomson scattering (TS): the small size of the laser beam (75 μm) means that only a (small) part of the radial distribution can be diagnosed. Figure 13a describes the experimental set-up for measuring the electron density along a surfatron plasma column using TS. The intersection of the laser beam and the focal spot of the triple grating spectrometer (TGS) (whose slit is parallel to the axis of the laser beam) defines the (small) detection volume of the TS. In this case, the TGS slit was focused on $r = 0$, ignoring the contribution of electrons from the rest of the radial electron density distribution.

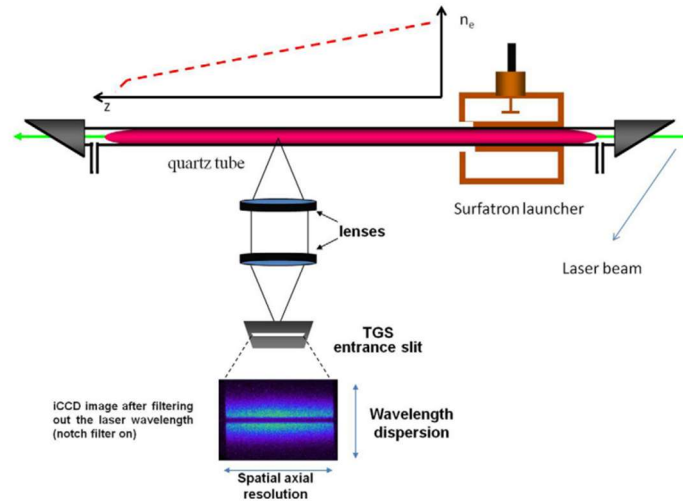


Figure 13a. Diagram of the surfatron plasma source and of the detection system for TS diagnostic showing how the triple grating spectrometer's (TGS) entrance slit is focused [25].

Figure 13b shows that beyond 40 mbars (30 Torr) in a tube of radius $R = 3$ mm the axial distribution of the electron density of an argon surfatron plasma at 2450 MHz is no longer linear [24].

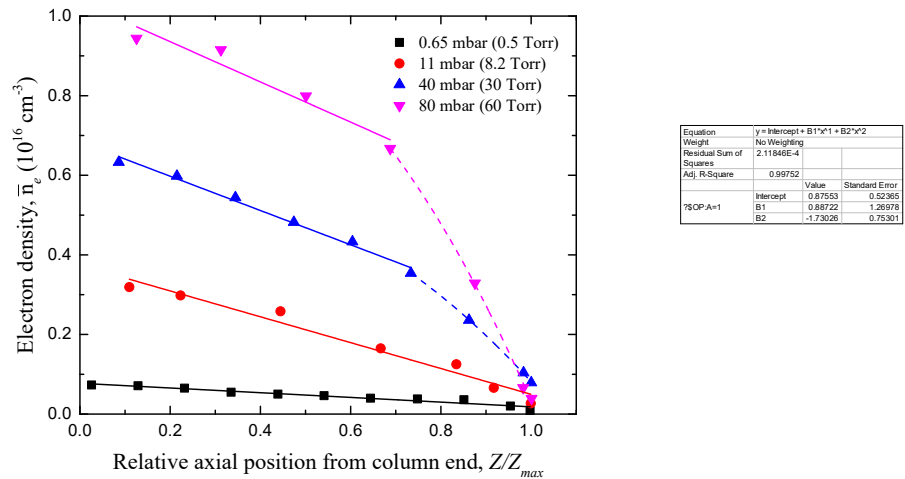


Figure 13b (foreign laboratory). Axial electron density distribution determined by Thomson scattering diagnostic of a surfatron plasma column maintained at 2450 MHz in argon at four gas pressures in a fused silica tube of $R = 3$ mm (adapted from [24]).

The loss of linearity marked by the axial decrease in electron density, as shown in Figure 13b, is due to the radial contraction of the plasma column, a contraction that becomes increasingly pronounced towards the end of the column (figure 9). If we consider that the (narrow) laser beam is directed towards a given point in this radial distribution of electrons other than its center, the intensity of the laser beam collected by the spectrometer, due to plasma column contraction, decreases towards the end of the column (in addition to its decrease in intensity due to the expected depletion of the TW power).

2.6.3. Underestimation of the electron density of the axial distribution provided by a Langmuir probe due to erroneous estimation of the ion saturation current density. The lowest electron densities reported in figures 11 and 12 are less than $\bar{n}_{e(\text{re})}$ (2), the minimum value of electron density for travelling wave propagation under low-collisional regime, indicated by the arrow outside the frame of figure 11. The validity of $\bar{n}_{e(\text{re})}$ as a travelling wave propagation threshold was verified using as a diagnostic tool for electron density the TM₀₁₀ resonant cavity (figures 2b and 6) as well as the axial phase variation (figure 8).

To sum up in a complementary way, the axial distribution of the electron density along the studied discharges is determined by the axial distribution of the power loss of the wave in relation to the electrons it heats. The slope of this distribution, as shown experimentally (Sec. 2), depends on the three operating parameters p , f and R and ultimately determines the average energy of the electrons.

Remark. An error during data processing falsely led to a deviation from the linearity of the axial distribution of the electron density in an earlier SWD recording (figure 7 in [14]) made at 915 MHz and 270 W in argon at atmospheric pressure: a downward curvature of the axial distribution of the electron density then appeared at the end of the plasma column. This behaviour is not compatible with the recording made under the same conditions at the higher power of 700 W, where the electron density is linear along the entire length of the plasma column. As it has been shown that the slope of the axial distribution of the electron density remains the same when the RF/MW power of the field applicator is increased or decreased (see figure 5 as an example), the curve at 270 W should rightly be linear along its entire axial length.

3. Key mechanisms dictating the linearity of the axial distribution of electron density in TWDs

The progress described so far in this paper has been achieved by exploiting the experimentally demonstrated linearity of the axial profile of the electron density. Further progress is possible by studying the reasons for this linearity, namely the stationary state stability condition of discharges supported by EM travelling waves, and by developing the conditions for electron heating.

3.1. The stability of discharges maintained by travelling electromagnetic waves, whatever their specific nature, requires the electron density to decrease monotonically axially.

In early studies of supposedly SW discharges [4], it had been assumed without theoretical support that the electron density $\bar{n}_e(z)$ along these discharges is proportional to the power dissipated by the wave at each point z , thus empirically relating the power attenuation coefficient $\alpha(z)$ to $\bar{n}_e(z)$ ⁷. It was Zakrzewski [27] who then demonstrated that to ensure a stable discharge (the production of charged particles is balanced by their loss), not only the power of the wave, but also the density of electrons along a long column of plasma must decrease monotonically. This comes from the following inequalities on power flow and electron density that [27]:

$$dP(z)/dz. d\bar{n}_e(z)/dz > 0 \text{ and } d\bar{n}_e(z)/dz < 0, \quad (3)$$

where z is evaluated from the start of the TWD. Analytical expressions for the proportionality between the wave power attenuation coefficient $\alpha(n)$ and the electron density as a function of axial position were then sought. One such possible relationship is proposed in [27]:

⁷ This empirical fact is taken into account in the article by Aliev et al. [26] without any specific physical justification (Sec. 4.1.2).

$$\alpha(n) = An^k \quad (4)$$

where k is an integer and A a constant, with the electron density n normalised to its value at the start of the TW sustained plasma column, n_{cs} . Recall the following expression [4]:

$$\frac{dn}{dz} = -2\alpha(n)n(z) \left(1 - \frac{n(z)}{\alpha(n)} \frac{d\alpha(n)}{dn}\right)^{-1}, \quad (5)$$

then from (4) and (5), there come:

$$\frac{n(z)}{n_{cs}} = \left(1 + 2An_{cs}^k \frac{k}{1-k} z\right)^{-1/k} = \left(1 + \frac{2k}{1-k} \alpha_{cs} z\right)^{-1/k} \quad (6)$$

$$\text{and } \frac{P(z)}{P_{cs}} = \left(\frac{n(z)}{n_{cs}}\right)^{1-k}, \quad (7)$$

where the normalised quantities n_{cs} , α_{cs} and P_{cs} are those at the start of the plasma column. Figure 14 is a graph of equation (6).

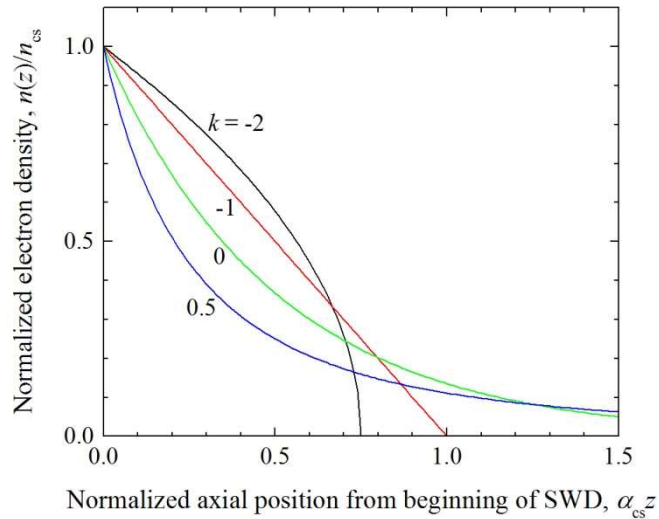


Figure 14 (foreign laboratory). Electron density as a function of axial position, as predicted by the *Zakrzewski criterion* to justify the stability of a long discharge (regardless of its end) maintained by a travelling EM wave. The two quantities n_{cs} and α_{cs} are normalised with respect to their values at the beginning ($z = 0$) of the TW plasma column, assuming $\alpha(n) = An^k$. The $k = -1$ curve corresponds to the linearly decreasing axial distribution of electron density, as observed experimentally, and documented in section 2.

Figure 14 shows that the axial profile of the electron density distribution, according to calculations from relationship (4), can either be concave ($k = 0.5$ and 0), linear ($k = -1$) or convex ($k = -2$), all of these possibilities for k strictly complying with the stability criterion $d\bar{n}_e(z)/dz < 0$ requiring $\bar{n}_e(z)$ to decrease monotonically. It should be noted that these axial electron density profiles are obtained for discharges maintained by travelling EM waves of any kind, i.e., without involving their specific dispersion properties, as well as independently of the features of the plasma columns produced. Among the various values of k in figure 14, only $k = -1$, as already mentioned, corresponds to the

observed axial distribution. This single value of k results from what happens in the transient period preceding the stationary state (see further below).

The arguments put forward by Zakrzewski assume that the SW axial field intensity E_0 is constant along a long SW plasma column [27], which justifies that the axial distribution of electron density decreases linearly, wrongly suggesting at the same time that E_0 should drop sharply at the end of the column. Instead, we experimentally observe a sudden increase in the intensity of the E_0 field at this point and in its immediate vicinity [28]. In fact, this deviation from $E_0 = \text{constant}$ at the end of the column is compensated for by a decrease in the cross-section S of the plasma (Sec. 3.3 below) so that the linearity of the axial electron density of the plasma column is always maintained to the end, as observed throughout Section 2.

The fact that $k = -1$ is reached experimentally (axial linearity of the electron density) is linked, as mentioned, to the transient period that precedes the stationary state. At the start of this period, the travelling wave from (for example) the surfatron towards the end of the column produces distinct plasma clusters [29]. The evolution towards discharge stability leads to a monotonic decrease in electron density towards the end of the plasma column, so that the initial plasma segments merge to form a single plasma column of decreasing electron density. As the possible axial electron density profiles other than $k = -1$ exhibit curvature, their corresponding axial gradient favours electron transport, eventually eliminating these curvature gradients in favour of an axial gradient that locally eliminates further reflection, i.e., leads to a linearly decreasing axial electron density distribution.⁸

3.2. Derivation of the relationship linking the TW power attenuation coefficient $\alpha(z)$ and the electron density $\bar{n}_e(z)$ assuming that only electrons are heated up by the TW field.⁹

Considering that the travelling wave propagates in the $-z$ direction ($z = 0$ is now the plasma column end in this model), the basic power flow equations are then:

$$\alpha(z) \equiv \frac{1}{2P(z)} \frac{dP(z)}{dz} \quad (8)$$

and

$$L(z) = \frac{dP(z)}{dz} \quad (9)$$

where $\alpha(z)$ defines the attenuation coefficient of the travelling wave power flow along z , and $P(z)$ is this power flow¹⁰. $L(z)$ is defined as the power lost by the electrons per unit length due to collisions of all kinds at z , compensated by dP/dz , the absorbed wave power. $L(z)$ can then be expressed as [12]:

$$L(z) = \bar{n}_e(z)\theta(z)S(z) \quad (10)$$

where θ is the power absorbed per electron [9] and S the plasma cross-sectional area, both depending a priori on z but their product being axially constant as imposed in (13) further on.

The experimentally observed axial distributions of electron density displayed in section 2 unambiguously suggest as a starting point that:

⁸ Assuming that the discharge tube is longer than the plasma column produced.

⁹ The analytical derivation that follows (inspired from [4]) is proposed here for the first time.

¹⁰ Note that this demonstration does not specify in which medium(s) the wave propagates and loses its energy.

$$\bar{n}_e(z) = n_0 + bz \quad (11)$$

where n_0 is the electron density at the plasma column end¹¹ and $b \equiv \frac{d\bar{n}_e}{dz}$, the (constant) slope of the axial distribution of electron density. Expressing (10) fully as:

$$L(z) = (n_0 + bz)\theta(z)S(z), \quad (12)$$

then from (9) $P(z)$ can be formulated as an integral over $L(z)$ in the form:

$$P(z) = \theta S \int_0^z (n_0 + bz) dz + P_0. \quad (13)$$

As indicated, the values of θ and S possibly vary along the plasma column, but their product θS cannot: otherwise, $P(z)$ in (13) would vary with $S(z)$, which opposes the experimentally demonstrated independence of electron density (11) from plasma diameter variations along the column (Sec. 3.3 further). After integration and calling on (8) and (13), one gets:

$$P(z) = (n_0 z + \frac{1}{2} b z^2) \theta S + \frac{n_0 \theta S}{2\alpha_0}, \quad (14)$$

identifying the power flow remaining at the column end:

$$P_0 = \frac{n_0 \theta S}{2\alpha_0} \quad (15)$$

and finally:

$$P(z) = \left(\frac{n_0}{2\alpha_0} + n_0 z + \frac{1}{2} b z^2 \right) \theta S. \quad (16)$$

From (8) and (16) and remembering that the product θS is independent of z , there comes:

$$\alpha(z) = \frac{n_0 + b}{\frac{n_0}{\alpha_0} + 2n_0 z + b z^2}. \quad (17)$$

Relation (17) can be also written as:

$$\alpha(z) = \frac{b \bar{n}_e(z)}{\bar{n}_e(z)^2 + c} \quad (18)$$

where:

$$c = n_0 \left(\frac{b}{\alpha_0} - n_0 \right). \quad (19)$$

Posing $c = 0$ (see below):

$$b = n_0 \alpha_0 \quad (20)$$

¹¹ The end of a TWD, under low-collision regime, has been shown above to be characterized by an electron density $\bar{n}_{e(\text{re})}$ (2) below which wave propagation stops.

then from (18):

$$\alpha(z) = \frac{b}{\bar{n}_e(z)} \quad (21)$$

Also, of b (11):

$$\alpha(z) = \frac{d\bar{n}_e}{dz} \frac{1}{\bar{n}_e(z)} \quad (22)$$

or equivalently:

$$\alpha(z)\bar{n}_e(z) = \frac{d\bar{n}_e}{dz} \quad (23)$$

where $\frac{d\bar{n}_e}{dz}$, recall, is experimentally constant till the very end of the plasma column (Sec. 2) and, therefore, such must be the product $\alpha(z)\bar{n}_e(z)$ all along the plasma column, unlike the result of model calculations where, for example, this product grows exponentially towards the column end [2].

The present derivation involves only the electrons of the discharge (as the wave power absorbing medium), but no other properties of the plasma. As for the posing of $c = 0$ in (19), it yields $\alpha(z) = \frac{b}{\bar{n}_e(z)}$ (21) which conforming with equation (4) written as $\alpha(n) = A/n^{-k}$ (to take account of the *discharge stability* criterion, Sec. 3.1) leads to $k = -1$, corresponding to the experimentally observed axial electron density distribution.

3.3. The independence of axial position of the product $\theta(z)S(z)$ is required to ensure the linearity of the axial distribution of electron density up to the end of the plasma column

The fact that the product $\theta(z)S(z)$ is axially constant is an essential (and original) feature coming out from our model (Sec. 3.2). To illustrate its significance, consider the case of a low-pressure TWD where the value of θ_A (absorbed EM power per electron) is experimentally constant throughout the plasma column, except at its end where it increases sharply, as depicted in figure 15a [28] (see [1] for detailed physical reasons); at the same time, the plasma radial luminosity, indicative of the plasma cross-sectional area S , contracts radially at the column end, as can be seen in the photograph (figure 15b). The product $\theta(z)S(z)$ in fact remains axially constant because the sudden increase observed in θ at the end of the column (figure 15a) is offset by the corresponding reduction in plasma cross-sectional area S , as can be seen in the photograph (figure 15b) as well as from the luminous diameter of the plasma column (figure 15c).¹²

All the theoretical work published to date has been wrong about the value of the axial electron density at the end of the plasma column, estimating or believing that it should decrease continuously: in fact, experimentally, after its linear decrease, the electron density drops abruptly to zero at the end of the column (cessation of the TW propagation). As for the role of the product $\theta(z)S(z)$ in this behaviour, it was ignored, most probably because no one has noticed the corresponding reduction in $S(z)$. This made it impossible to adequately resolve the problem raised by the sudden surge in E_0 (and θ) at the end of the column [28], given that experimentally this sudden increase in wave field intensity does not affect the rigorous linear decrease in electron density until the very end of the plasma column. This condition on $\theta(z)S(z)$ is essential to obtain

¹² Clearly a rigorous check on $\theta(z)S(z) = \text{constant}$ would necessitate determining $\theta(z)$ and $S(z)$ under the same operating conditions.

$\alpha(z)\bar{n}_e(z) = \frac{d\bar{n}_e}{dz}$ which leads to $k = -1$, i.e., for the axial distribution of the electron density to be linearly decreasing from the beginning to the end of the plasma column.

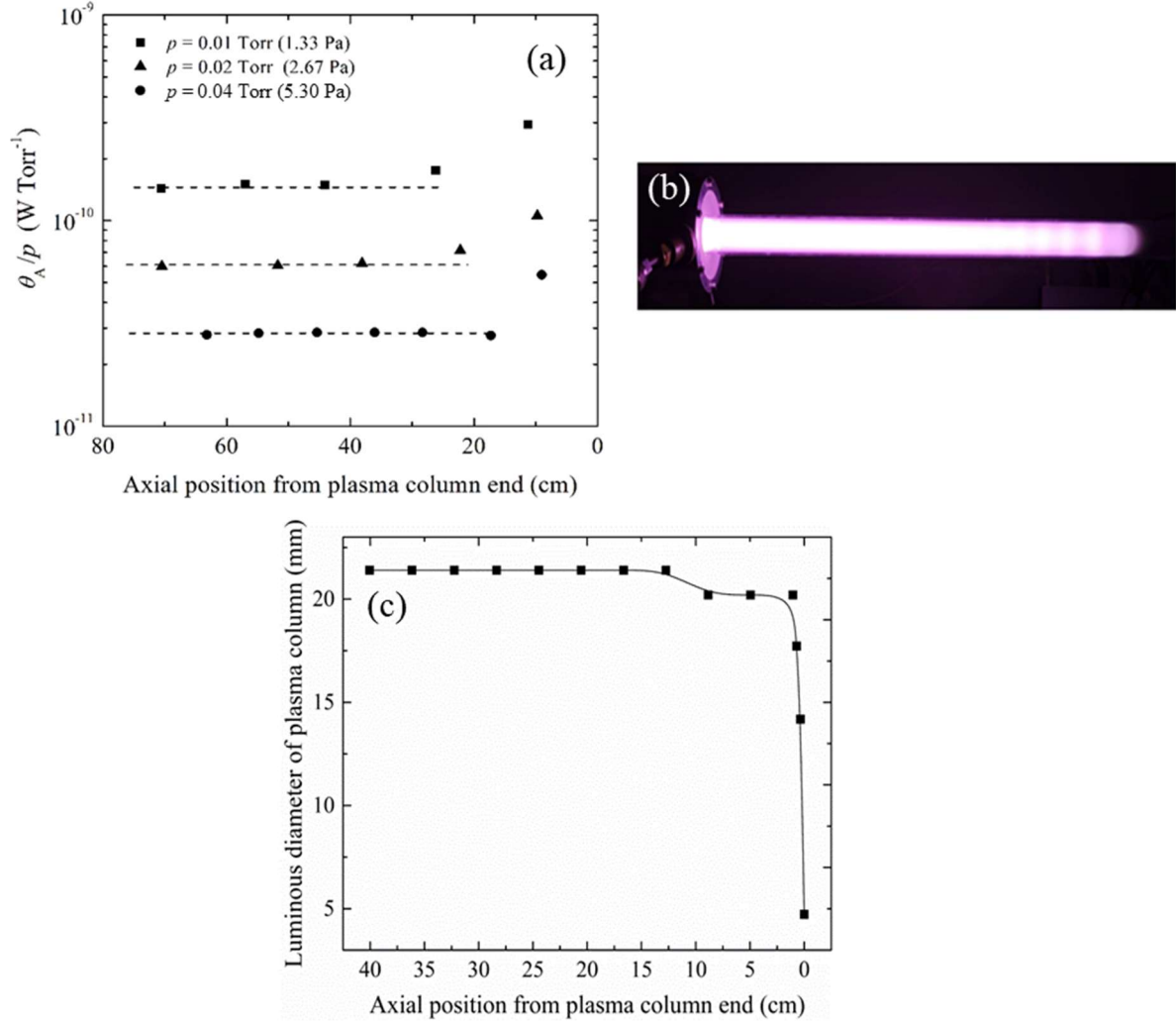


Figure 15: a) Measured values of θ_A/p as a function of axial position relative to the end of the TW plasma column sustained at 200 MHz in a tube with internal and external radii of 13 and 15 mm, for three different gas pressures p (low collision regime). For a given gas pressure, the power absorbed per electron θ_A does not vary with axial position except, at the end of the column [28]; b) photograph of an argon TWD at 0.05 Torr (6.7 Pa) sustained at 915 MHz in a tube with an internal radius of 10.7 mm. The TW runs from the left (surfatron gap) to the end of the plasma column on the right. The radius of the plasma column decreases at the end as it becomes rounder. The alternating variations in luminosity at the end of the column are due to the combined reflection of an azimuthally symmetric surface wave ($m = 0$) and a dipolar surface wave ($m = 1$): see Appendix C; c) measured luminous diameter (leading to S) of the plasma column indicating that it fills the discharge tube except at the very end of the plasma column where it decreases abruptly over about 10 mm.

3.4. The terminal part of any experimentally collected TW plasma column, however small, allows determining the true axial distribution of electron density over any length by linear extrapolation: an essential feature of TWDs.

This feature of TWDs (called SWDs in the literature) is well known and experimentally documented (for example, figure 5), and is valid whatever the operating conditions. The linearity of the axial distribution of the electron density follows from our representation of the wave power distribution as an energy conservation law linking the axial power expenditure of the wave and the corresponding heating of the electrons, throughout the plasma column, from start to finish (Sec. 2.6.1). This is because as the TW propagates it dissipates its power axially in a linear manner (to guarantee the stability of the discharge, Sec. 3.1) to the sole benefit of the heating of the electrons in the discharge gas, thus ensuring the ionisation of the plasma column. This phenomenon linking the attenuation of the wave and the resulting electron density is expressed by the relation $\alpha(z) = \frac{b}{\bar{n}_e(z)}$ (21). It is therefore one and the same mechanism that acts from the beginning to the end of the TW plasma column. None of the models published to date reproduce such overall behaviour. Indeed, these same calculations all show a more or less strong deviation from linearity at the end of the column, in contrast to linearity observed along the entire length of the TWD (Sec. 2).

It should be emphasized that the stability of a discharge sustained by a travelling wave does not depend on the specific nature of this wave, in particular its dispersion, and that relation (21) excludes any other possible dependence on the propagation medium. The travelling wave can only propagate outside the discharge tube and in the surrounding ambient air, otherwise its propagation through the plasma column would be attenuated, reflecting the properties of the latter: the attenuation coefficient TW, it is stressed, only serves to heat the electrons in the discharge gas, excluding any other type of power loss of the wave. It is in fact the electric field of the travelling wave (propagating outside the discharge tube) which penetrates inside the discharge tube, ionising the gas it contains.

4. Critical review of a selection of papers dealing with the modelling of the axial distribution of electron density along SWDs¹³

The fact that the electron density observed along a TWD decreases linearly whatever the operating conditions p , f and R (Sec. 2) is certainly intriguing, hence the great interest aroused among theorists: many saw in it the possibility of determining the relationship between the properties of the surface wave and those of the plasma column, since the majority belief is that there must be a dependence of the surface wave on the plasma, the surface wave being assumed to propagate in the three media of this tubular discharge. This commonly held (wrong) assumption is in fact the major concern that permeates our article.

These studies can be divided into two categories according to: 1) the dispersion of the surface wave is linked solely to the electron density of the plasma column, the value of which is fixed by the power of the wave absorbed axially; 2) one of the characteristic properties of the discharge is additionally imposed (in various ways) by the modeller.

4.1. The surface wave properties are determined (analytically or by numerical simulation) for a cold homogeneous plasma characterized by its relative permittivity. No discharge parameter is imposed besides the three operating conditions (p for N , f and R)

4.1.1 *Glaude et al.* [4] (1980) provide experimental results supplemented by numerical calculations. This pioneer paper paved the way for the study of the fundamental properties of surface wave sustained plasmas: not only does it describe the key attributes of these plasma columns, but it shows how the electron density $\bar{n}_e(z)$ (related to ω_{pe} in the real part of ε_p , [20], the relative permittivity describing the plasma) depends on the wave frequency $\omega/2\pi = f$ (present in

¹³ Which should be considered in fact as TWDs although identified as SWDs in all until now papers.

ε_p), on the internal radius R of the discharge tube through $S = \pi R^2$, and on the electron-neutral collision frequency for momentum transfer ν (the imaginary part of ε_p). A remarkable result, identified experimentally, is that the number of electrons $\bar{n}_e(z) S \Delta z$ in the cylindrical section of small axial extension $z, z + \Delta z$ is proportional to the power $P_a(z)$ absorbed within it according to:

$$\bar{n}_e(z) S \Delta z \theta = P_a(z) \quad (24)$$

where θ is the power absorbed per electron [9] (and not its inverse $1/\theta$ as initially in [4]). Since θ is assumed axially constant here, considering two successive short cylindrical plasma segments at z_1 and z_2 , one can thus write:

$$\theta = P_a(z_1)/\bar{n}_e(z_1) S \Delta z_1 = P_a(z_2)/\bar{n}_e(z_2) S \Delta z_2 \quad (25)$$

where the values of electron density and absorbed wave power of the first cylindrical segment gathered from measurements allow the iterative calculation process to begin for the second segment since the value of θ has initially been determined (see [4] for the complete procedure).

By keeping constant the three parameters ω, S and ν defining the operating conditions, calculations generate a linear axial distribution of the electron density, except at the end of the column where "numerical oscillations" are reported. Furthermore, similar calculations but varying one of the parameters ω, S and ν at a time also lead to a linear axial distribution of electron density (except again at the end of the column): the slope of these distributions is found to increase with wave frequency f , collision frequency ν and decrease with the discharge tube internal radius R (via S). Finally, the authors show that, given $\alpha(z)$, the attenuation coefficient of the surface wave power, the gradient of the axial electron density found to be given by:

$$dn/dz = \alpha n, \quad (26)$$

is approximately a constant, except at the end of the column where α diverges.

Finally, an expression to remember from [4], much used in later publications:

$$dn/dz = 2\alpha n / (1 - n da/(a dn)). \quad (27)$$

The presentation of these authors cannot be considered as a real model because physical explanations are missing: it is rather an empirical description based on the observed constancy of θ [9]. In this respect, the density of the electrons is deemed sufficient by itself to characterize the plasma column, no other discharge properties are mentioned indicating that the question of a possible influence of the plasma column on the surface wave has not yet been raised. Finally, since this work does not result in a linear distribution of electron density over the entire length of the plasma column as observed, it should be considered incomplete.¹⁴

4.1.2 *Aliiev, Boev and Shivarova* (1982) [26] were the first to propose an analytical model reproducing a plasma column maintained by an EM surface wave. Their only imposed link between the wave and the plasma is the assumed/observed proportionality of the electron density with the absorbed wave power in each axial position of the column; no other properties of the plasma column are considered. The following presentation copies literally the first lines of their paper, highlighting their contribution (CGS units are used).

¹⁴ The problem of numerical divergence at the end of the plasma column is solved analytically in our model in section 3.2 and based on our experiment in section 3.3, which requires to consider that the product $\theta(z)S(z)$ is independent of z .

"Consider a weakly damping electromagnetic wave of TM type having both axial and radial electric field components E_z , and E_r , respectively, and an azimuthal magnetic field component B_ϕ . The slow variation along the z -coordinate of the seek for quantities is determined by the energy conservation relation of the surface wave:

$$\frac{d\bar{S}(z)}{dz} = -\bar{Q}(z) \quad (28)$$

where \bar{S} (here) is the SW power flow averaged over a wave period:

$$\bar{S} = \frac{c}{8\pi} Re \int_0^{2\pi} d\phi \int_0^\infty r E_r(r) B_\phi^*(r) dr \quad (29)$$

and Re and $*$ mean the real part of and the complex conjugate of a quantity, respectively, c being the speed of light. As for the value of \bar{Q} , the Joule collisional heating losses in the plasma column per unit axial length, it is given by:

$$\bar{Q} = \frac{1}{2} \int_0^R r dr \int_0^{2\pi} d\phi (Re \sigma) |E|^2 \quad (30)$$

where σ is the conductivity of the low-temperature plasma. Further it is assumed that the frequency of the elastic electron-neutral collisions does not exceed the surface wave frequency ($\nu < \omega$), thus neglecting collisional damping. The energy conservation law is expressed, for simplicity, in the thin cylinder approximation (the plasma cylinder of radius R , located in vacuum, is smaller than the skin depth). E_z is the axial electric field component which in the case of the thin cylinder has a constant value over the plasma column cross-section and exceeds considerably the radial electric field component. The plasma (relative) permittivity:

$$\epsilon_{p1} \approx -(\omega_{pe}^2 / \omega^2) \quad (31)$$

is negative with an absolute value much greater than unity (according to the case of surface waves in the thin cylinder approximation). This condition allows neglecting in the power flow the contribution of the wave propagation in the plasma (the obtained general expression for \bar{S}_z shows that in the thin cylinder case only the power flow forward in the z -direction is considerable and this flow is in vacuum" (end of first citation) [26].

The energy conservation relation (28) is adapted for azimuthally symmetric waves in the thin cylinder approximation. Going on with their analysis, as mentioned, the authors take advantage of the experimental fact that the local value of the electron density (expressed through the plasma relative permittivity) is proportional to the wave power released locally along the plasma column [4], which they expressed as¹⁵:

$$|\epsilon_{p1}| = \beta E_0^2 \quad (32)$$

where β is in their paper some constant and " E_0 is the axial electric field component which in this case of the thin cylinder has a constant value over the plasma column cross-section and exceeds considerably the radial electric field component" [26].

The authors use the SW dispersion relation of a homogeneous cold plasma column surrounded by vacuum whose electron density is provided by (31) and (32).

The analytical results for the axial electron density distribution along the gas discharge axis is finally [26]:

¹⁵ Corresponding to the volume recombination regime.

$$n_e(z) / n_e(0) = 1 - z / L \quad (33)$$

where:

$$L = (R/v\omega)\bar{f}(12\pi e^2/m) n_e(0) \quad (34)$$

Is, here, the length of the produced plasma column, $n_e(0)$ is the electron density value at $z = 0$ where the surface wave generator is situated¹⁶, $\bar{f} = 0.16$ is a wave dispersion average value and m (here) is the electron mass [26]. In the end, the gradient of the electron density distribution can be expressed as:

$$\frac{dn}{dz} = -(v\omega / R)(\bar{f}^{-1}m/12\pi e^2) \quad (35)$$

where the authors assume that the electron-neutral collision frequency ν does not vary along the plasma column which allows them to preserve the observed axial linearity of the electron density all along the plasma column. Considering, in this condition, ν instead of the gas density N as an operating condition (see footnote 3) amounts to the same thing from a calculation point of view.

"The initial value of the wave power (at $z = 0$) determines the length L of the plasma column but it does not influence the electron density axial profile" [26]. Comparison with the experiment showed that the calculated properties of their plasma column, despite the very restrictive assumptions of the model, gave a correct picture of wider operating conditions. The analytical result they obtained corresponds perfectly to the linear axial distribution of electron density observed along the entire length of the plasma column as per Sec. 2.

4.1.3 *Aliev, Boev and Shivarova* paper's (1984) [30] is again based on the thin plasma cylinder approximation, but this time enclosed in a dielectric tube. In a thin plasma cylinder, as mentioned in the preceding section, it is the axial component of the wave electric field (with a constant value on the plasma radial cross-section) that ensures the heating of the electrons in the discharge gas. The authors once more assume the proportionality of electron density with the wave power absorbed at each axial position of the column. The dispersion characteristics of the (TM mode) surface wave and the axial and radial components of their field are determined in a cold homogeneous plasma characterized by its relative (cross-sectional average) permittivity ϵ_{p1} (32). They also calculated the respective contribution of ambipolar diffusion and volume recombination to charged particle recombination. Although the recombination effects on the discharge are very different in these two cases, the gradient of the axial density of the electrons is nevertheless found identical in its form to (35).

4.2. Cases where characteristic elements of the SW plasma column are introduced into the wave equations to tentatively determine the influence of these properties on the axial distribution of the electron density

¹⁶ Aliev et al. [26] were not aware at the time that the actual SWD was not immediately starting at the field applicator gap, which, as documented much later (2019), results in an antenna-like radiation region [7]. Nevertheless, the possible existence of a region with properties different from those of the linear axial distribution of electron density (SWD) was reported as early as 1980 (see figure 3 in [4]), but without due explanation.

Our analytical description of the axial distribution of the electron density in section 3 clearly puts forward the fact that the axial electron density is proportional to the power dissipated by the wave as it travels (Sec. 3.2). The heating of the electrons (ionisation) in the discharge gas, as we have mentioned, ultimately exhausts all the power of the travelling wave, without depending on the properties of the plasma column. When examining the papers below, remember from Sec. 2 that the experiment indicates that the linearity of the electron density profile is not affected or lost as a result of any variation or combination of variations in the three operating parameters of the TWD, namely N (represented by p), f and R .

Our new interpretation of the discharges referred to in the literature as SWDs is based above all on compliance with the stability conditions (stationarity) for discharges maintained by the propagation of an electromagnetic wave. The stability of these discharges requires the wave feeding them to be a travelling wave, without any implication as to its specific dispersion properties. This wave is in fact first and foremost a wave that distributes its energy to the electrons and to them alone; this wave in the end ensures an axial distribution of the electron density that decreases linearly from the beginning to the end of the column. This wave, generally azimuthally symmetric, propagates, in our view, only in the ambient air (vacuum) surrounding the discharge tube. In contrast as currently understood, the 'surface wave' propagates along the plasma column and its discharge tube, which we maintain is not the case.

4.2.1. *Mateev, Zhelyazkov, Atanassov* (1983) [31] studied analytically the axial electron density distribution of SWDs in a similar initial manner to that of Aliev et al. [30]: the plasma column is represented by the relative (complex) permittivity of a cold homogeneous plasma embedded in vacuum. The wave energy dissipated into the medium heats the electrons which ionize the neutral gas, thus sustaining the plasma column; Maxwell's equations are developed in the electrostatic (slow wave) approximation with applying the standard boundary conditions for the field components.

An original part of their contribution lies in the introduction of "universal" curves, $\bar{n}_e(\zeta)$ and $E^2(\zeta)$, resorting to a dimensionless axial space coordinate $\zeta = v z / \omega R$, which aggregates the values f , v and R , i.e., the three parameters defining the operating conditions. Another new aspect brought out by these authors is to consider that the influence of electron density on discharge properties differs between low and high gas pressure regimes:

i) "under low pressures, electron density is proportional to the absorbed wave power per unit length. This case occurs when the average lifetime of the charged particles is determined by their diffusion to the discharge tube walls". To a first approximation, they give a relationship for the axial gradient of the electron density like equation (35) of Aliev et al., namely:

$$\frac{dn}{dz} = 0.73 \times 10^{-8} \frac{\omega}{2\pi} \frac{v}{R} (cm^{-4}); \quad (36)$$

ii) at high pressure, electron density is proportional to the total energy of the wave field per unit length. This occurs when the average lifetime of the charged particles is defined by bulk (volume) recombination.

In both cases of pressure, the plotted axial distribution of the electron density deviates, although very little, from the perfect linearity showing a slight overall circular curvature extending from the beginning to the end of the plasma column. At the end of the column, a noticeable downward curvature of the electron density axial distribution is additionally observed, which the authors justify by the corresponding increase in the intensity of the E wave field.

4.2.2. *Zhelyazkov, Benova, Atanassov* (1986) [32] take up the theoretical approach of Mateev et al., which they claim is limited by the electrostatic approximation (Sec. 4.2.1), and extend it by considering a complete EM description of the SW field components: to follow the evolution of this

correction to the model, they introduce the parameter $\sigma = \omega R/c$ where $\sigma = 0$ corresponds to the electrostatic approximation. They find that the higher the value of σ , the more linear the axial distribution of electron density, in fact the overall slight deviation from linearity disappears above $\sigma = 0.2$; however, the downward curvature already noted at the end of the plasma column in Mateev et al. (Sec. 4.2.1) persists. At the same time, the authors follow up (for different values of σ) the comparative effect of the loss of charged particles by diffusion and that of volume recombination on the axial distribution of electron density, showing that these losses do not influence its linearity (fixed by the value of σ), but rather modify the value of its slope.

In the end, it seems that a full EM treatment of the SW is essential to ensure recovering analytically the linearity of the electron density along the plasma column.

4.2.3. *Aliev, Maximov, Schluter, Shivarova (1995)* [33] wanted to demonstrate the preponderance of resonant absorption of the surface wave power in SWDs compared with collisional absorption. To simplify the calculations and get straight to the point, the authors consider a plasma slab instead of a plasma column. Recall that resonance absorption requires the existence of a transition region in which there is a longitudinal (axial) gradient of electron density that allows the resonance condition $\omega = \omega_{pe}$ to be reached at a certain point z along this gradient; according to them, there would be resonance at the beginning and end of the plasma slab. However, such a situation does not exist because both at low pressure and at atmospheric pressure (Sec. 2), the axial electron density profile of a SWD is always experimentally linear along the entire plasma slab (column), and there is therefore no specific transition region either at the beginning or at the end of the plasma column.

4.2.4 *Aliev, Ivanova, Moisan, Shivarova (1993)* [34] proposed an analytical derivation based on the thin-cylinder approximation (the E_r field component can be neglected before E_z ¹⁷) for a cold, weakly collisional homogeneous plasma supported by a SW, as first developed by Aliev et al. (Sec. 4.1.2), with the main aim of extending their previous results standing for volume recombination (32) to the (ambipolar) diffusion regime. Various approximations and assumptions are made to obtain analytical expressions for $\frac{d\bar{n}_e}{dz}$ and $E(z)$. The model clearly distinguishes the respective roles of the charged particle recombination regime, the influence of the wave dispersion features and the discharge operating conditions:

- i) the charged particle loss mechanism appears as a numerical factor α determining the slope of the always linear axial distribution. The slope of the axial distribution of electron density is less in the case of volume recombination than for ambipolar diffusion in given discharge parameters;
- ii) the wave dispersion turns up as an average value $\langle f \rangle$ taken over a limited interval of the electron density;
- iii) the discharge operating parameters are taken into account via the term $v\omega/R$.

Following these various approximations, the resulting axial distribution of electron density is linear, in line with experience (Sec. 2), i.e., (CGS units)¹⁸:

$$\frac{d\bar{n}}{dz} = -\frac{1}{\alpha} \frac{v\omega}{R} \frac{m_e}{4\pi e^2} \frac{1}{\langle f \rangle}, \quad (37)$$

except at the very end of the plasma column where the electron density drops rapidly, which the authors considered out of the region of validity of the thin cylinder approximation. Note that the slope of the electron density distribution is related to the wave dispersion through the average

¹⁷The only wave field component in the plasma column is then $E_z(r)$, which is about radially constant (large skin depth, as demonstrated in Appendix C, paragraph d).

¹⁸ It excludes the very end of the column.

value $\langle f \rangle$, allowing the authors to claim that the SW propagation characteristics and the axial distribution of plasma density are interrelated.

4.2.5. Kovačević, Kuzmanović, Milosević, Djordjevich (2021) [15] proposed to analytically recover the axial electron density distribution using the so-called *square-root analytical approximation* of the SWD dispersion relation (introduced by Babović et al. [35]). It amounts to limiting calculations of the dispersion relation to the case $\beta R < 1$ where β (here) is the SW wavenumber: this approach facilitates the determination of the wave power attenuation coefficient $\alpha(z)$ by "avoiding the more difficult to handle cluster of Bessel functions of different types, orders and arguments". Using this approximation, they obtain axial distributions of the electron density that are linear from the beginning to the end of the plasma column. However, the physical significance of the $\beta R < 1$ approximation, which is somehow restrictive, is not discussed.¹⁹

The authors also wanted to examine the contribution of losses related to the dielectric permittivity of the tube and its thickness, which increase significantly with the frequency of the wave field²⁰ and the tube thickness. They therefore consider that, in addition to collisional losses, $\alpha(z)$ must include the dielectric losses of the discharge tube material, which as they mention could possibly affect the linearity of the axial distribution of the electron density. Their calculations in that respect show that linearity is 'a good approximation' insofar as R_{oi} , the ratio between the outer and inner radius of the tube, is less than 1.5, whereas for a thicker tube, the axial distribution of electron density should become increasingly parabolic with R_{oi} .

It is possible to look for these features experimentally, using tubes with particularly thick walls (tubes with an external radius of 8 mm and an internal radius of less than 1 mm in figure 4) or when the frequency of the travelling wave is increased, for example from 915 MHz (figure 4) to 2450 MHz (figure 7): in any case, the observed axial distributions remain linear. Since we now consider that the travelling wave propagates only in the vacuum (air) surrounding the discharge tube, it is normal for it not to be attenuated by the dielectric tube, as observed; on the other hand, the intensity of the electric field component of the travelling wave, which heats the electrons in the discharge gas, should be lowered as it passes through the dielectric wall of the tube.

4.2.6. Gordiets, B., Pinheiro, M., Tatarova, E., Dias, F. M., Ferreira, C. M., and Ricard, A. (2000) [23] consider that the vibrational and rotational excitation levels specific to molecular discharges, because they are added to those of atomic discharges, should modify the SW power flow to the point where it no longer leads to a linear axial distribution of the electron density. In fact, their corresponding calculation does show a significant deviation from the linearity of the axial distribution of the electron density (dotted line in figure 12), but this is not what is found experimentally since SWD discharges of N_2 (figure 11) and H_2 (figure 12) remain linear: this result is again consistent with our assertion that the travelling wave does not interact with the plasma column since it does not propagate in this medium.

4.2.7. Aliev, Yu. M., Maximov, A., Ghanashev, I., Shivarova, A., and Schlüter, H., (1995) [38] focused their attention on the fast EM wave (speed of propagation close to that of light) appearing at the output of the field applicator and up to a certain distance from it.

¹⁹ Their approximation calling for $\beta R < 1$ makes that it avoids considering the real end of the column skipping the problem of the downward curvature appearing in the calculated axial distribution of electron density.

²⁰ As an example, the percentage of dielectric loss on total losses (including conductors) at different frequencies of polyethylene ($\epsilon_g = 2.3$) in a coaxial cable at 100 MHz is 12%, at 1 GHz 29% and at 10 GHz 57% [36].

The nature of this wave was however misinterpreted by the authors as a variant of a SWD: this fast EM wave is in fact imposed by the field applicator then behaving as an antenna and, as such, giving rise to a space wave (meaning unguided and with a variety of radiation lobes) [7]. The shape of the recorded axial profile of the electron density of this fast wave varies significantly with the frequency of the EM field: for example, at 27 MHz (figure 1), it appears linear, while at 360 MHz, it can be described as somewhat quadratic, as shown in figure 2a before the linear axial distribution of the electron density characterizing a SWD (actually a TWD) appears. It was not until 2019 that the nature of this space wave was clearly documented experimentally, and thus associated with the role of the electromagnetic field applicator as an antenna [7].

4.2.8. Zhelyazkov and Atanassov [2] have written an exhaustive (122 pages) and remarkably well-constructed (like a textbook) report describing the axial distribution of the electron density of plasma columns driven by allegedly electromagnetic surface waves (meaning waves propagating in both the plasma column and the dielectric tube). Their main concern is the theoretical description of these waves and the plasma columns they produce. The report is accordingly divided into topics that characterise, on the one hand, the surface waves, including different possible modes of propagation (azimuthally symmetric and dipolar, noted $m = 0$ and $m = 1$, respectively) and, on the other hand, the structure, and properties of the plasma column they supposedly create; they also consider the action of a constant and homogeneous external (static) magnetic field on the EM surface waves. In each of these sections, the development of the subject follows a chronological order, sometimes accompanied by contributions from Zhelyazkov and Atanassov themselves.

Some of their comments shed further light on the subject by clearly identifying/summarising the main issues involved:

1) They divide the different aspects of the modelling of SWDs into three categories: (i) "approaches in which the surface wave and the plasma column are coupled; (ii) approaches that ignore the wave aspect of the problem but deal in detail with the equilibrium of charged particles in the plasma in the presence of an HF field (generally assumed to be uniform); and finally, (iii) approaches that focus on the propagation and attenuation characteristics of the wave and its power transfer to the plasma, but pay little attention to the equilibrium of the charged particles" [2].

Quoting again Zhelyazkov and Atanassov:

2) "The axial gradient of the electron density is entirely determined by the discharge conditions (as defined by Moisan and Zakrzewski [12]), i.e. the composition and pressure of the gas, the dimensions of the discharge tube and metal enclosure (if any), the permittivity of the tube, the strength of the applied static magnetic field, the magnetic induction B_0 , the mode and frequency of the wave; the electron density gradient does not depend on the power of the HF wave, which is then considered as a condition separate from the discharge conditions";

3) "a simple model for HF discharges produced by travelling electromagnetic waves is based on the assumption that the treatment of the physical processes occurring in the discharge can be divided into two separate parts: the first concerns the maintenance processes within the discharge; the second, the electromagnetic behaviour of the HF waves sustaining the plasma";

4) "the local wave dispersion relation is assumed to be linear as far as the field intensity is concerned. This validity was checked by Zakrzewski et al. [39] up to high wave power levels inclusive. Increasing the surface wave power density (in diffusion regime strictly) leads to a plasma density increase, not to an increase of the wave amplitude into the plasma".

This comprehensive (and didactic) report on SWD work is, however, limited to papers published up to 1995 and at low gas pressure. At that time, the existence of the antenna-like radiation zone of the field applicator, as mentioned, had not yet been examined (2019) experimentally (and explained) [7], while the experimental data on SWDs at atmospheric pressure were still little known due to their first publication (1990) in a "confidential" journal [14].

4.3 Comments on the articles reviewed. The term "approximately linear" or its equivalent is used in several articles to characterise the behaviour of an axial distribution of electron density that appears to be linear: in fact, in no case have these authors attempted a linear least-squares regression on their experimental data, which is what has been done in all the figures in section 2 representing the axial distribution of electron density. Furthermore, in none of these articles is it suggested that the linearity of the axial distribution of electron density is in fact a reflection of the linear decrease of the axial flow of wave power, which we have shown to be determined by the stability condition acting on any discharge maintained by a travelling electromagnetic wave. Consequently, all these papers ignore, moreover, that it is the same wave energy flow mechanism that governs the entire plasma column length (Sec. 3.4), explaining their admission of a different column end: apart from Kovačević et al. (4.2.5), the end of the plasma column obtained by modelling is never clearly linear and rather curved downwards.

5. Summary, discussion, and conclusion

5.1. Summary

The starting point for our modelling was the hypothesis, suggested by experiment, of a linear decrease in electron density along the plasma column from start to finish: it was therefore necessary to validate the extent of this observed characteristic and to provide explanations when this behaviour was not respected. It turned out that a non-linear axial distribution of the electron density of the plasma column does indeed appear when there is radial contraction of the plasma column and that, at the same time, not all the electrons in their radial distribution (at each axial position) are taken into account by the electron density diagnostic technique used: this is the case, for example, when the electron density is determined by Thomson scattering where the laser beam, limited in size, only probes a (very) small part of the radial distribution of electrons. Apart from this case, the examination in section 2 of an extremely wide range of operating conditions (N (or p), f and R) did not identify a single case where the linearity of the axial electron density distribution of the plasma column was challenged. In addition, to strengthen this study, for each of the axial electron density distributions presented, we checked the accuracy of the lines drawn from the experimental points using the well-known statistical method of least-squares regression.

A decisive element in the present model is the Zakrzewski criterion which states that the maintenance of a column of plasma by any EM travelling wave (TW) necessarily gives rise to an axial distribution of the electron density decreasing monotonically. Several axial distributions of electron density behaving in this way are in principle possible, as the calculation shows. In this respect, the examination of the transient period preceding the stationary state represents a breakthrough. It ensures that, after numerous reflections of the electromagnetic wave aimed at eliminating local gradients in electron density along the plasma column, a monotonic axial decrease in electron density is obtained: only the linear axial distribution of electron density remains once the stationary state is reached. Furthermore, it seems that the application of this stability condition does not depend on any dispersion property of the EM wave, which means that the wave feeding the plasma column does not interact with it, thus eliminating a point of disagreement with the proponents of SWDs.

The linearly decreasing axial distribution of the electron density reflects, as shown for the first time in the current paper, the axial dissipation of the wave's power in favour of the heating of the (only) electrons which, through the subsequent ionisation of the discharge gas, sustains the plasma column. In other words, the power attenuation coefficient $\alpha(z)$ of the wave, managing its power transfer, depends solely and completely on the electron density in $\alpha(z) = \frac{b}{n_e(z)}$ (21). There is therefore no power in reserve for further wave propagation, for instance, along the discharge tube and plasma column. It can therefore be concluded that the travelling wave, azimuthally symmetric in most cases (figure 14 in [48]), propagates only in a vacuum around the outer wall of the discharge tube.

In the case of the plasma produced by the TIAGO torch (Appendix B), the electron density observed along the plasma filament is first, at about 2 mm from the nozzle, that corresponding to the contribution of the antenna-type EM radiation zone. This is followed by the dart, a linearly decreasing distribution of electron density, as would be expected in the case of a TWD. The similarity of the axial distribution of electron density observed in the two cases confirms our identification of the TIAGO plasma nature and origin.

5.2. Discussion

Several issues addressed in this report merit further investigation. Firstly, the fact that in the weakly collisional regime ($v/\omega \ll 1$), the observed travelling wave ceases to propagate at the axial position where the electron density corresponds to what has been predicted theoretically in the case of a surface-wave plasma (the wave then propagating along the plasma column, not in a vacuum) at the cut-off value of the latter: this mechanism needs to be analysed and described in more detail.

Other points must be studied or better documented: i) the examination of what happens at the end of these plasma columns with the sudden increase in the electric field strength and its compensation, as we suggested, by the decrease in the plasma cross-sectional area, needed to guarantee the linearity of the axial distribution of the electron density; ii) the detailed time evolution of the electron axial density during the transient period, which leads in the stationary state to a unique linear distribution of the decreasing electron density along the axis; iii) the radial contraction of the plasma column under various operating conditions, including the formation of multiple filaments; iv) the quantity and nature of the discharge gas, which would be better represented, in our view, by its density N rather than the pressure p : it requires an analytical derivation of (1).

5.3. Conclusion

That paper established that the linear decrease in electron density observed along the plasma column sustained by a travelling EM wave is due to the dissipation of the wave power in favor of the heating of the sole electrons in the discharge gas, to the exclusion of other wave losses: this is the central point of our model. This energy transfer correctly reproduces the entire axial distribution of the electron density of the plasma column, from start to finish, including at its end, thus eliminating the-end-of-column problems (loss of linearity) encountered in all the papers published to date.

Our model goes against the idea of a surface wave propagating along the plasma column, and therefore dependent on the plasma column. In our view, as mentioned, the travelling EM wave responsible for maintaining the plasma column propagates only in the medium outside the plasma tube and its energy balance is strictly linked to the heating of the gas electrons by the electric field component of the EM wave. Finally, the analytical treatment that we have developed turns out to be entirely linear, in contrast to the corresponding many papers articles which claim that some non-linearity is related to electron density.

The availability in the laboratory of plasmas maintained by RF and MW TWs provides a unique, reproducible, and energy-efficient plasma medium which, combined with in-depth knowledge of their mechanisms, makes them a powerful research tool for developing new applications in a wide range of fields. In that respect, the flexibility and variety of their operating conditions means that there is no need to modify the discharge configuration, which is the case for all other types of RF and MW discharges when wanting to cover a wider range of operating conditions.

Appendix A: six different measurement techniques have been used to determine the axial distributions of electron density of the TWDs shown in this document

-1 The first method used at UdeM to obtain the axial distribution of electron density involved passing the discharge tube through the central hole of a flat (narrow width) cylindrical resonant cavity operating in the TM_{010} eigenmode. The plasma is represented by its equivalent (relative) permittivity, the value of which can be calculated and/or calibrated with the shift in the opposite direction of the observed resonance peak (on the screen of an oscilloscope) relative to low-loss dielectric liquids of known permittivity, for example, benzene. By varying the RF/MW power, which determines the length of the plasma column, the different segments of the plasma column pass successively through the cavity: the frequency shift of the resonance peak relative to that without plasma, which is greater the higher the value of the electron density, is recorded as a function of the plasma column end. The axial distribution of the electron density is then reconstructed, segment by segment [4]. A variant of the method involves calibrating the intensity of the light emission from a few segments of plasma in the cavity with the corresponding electron density, then recording the intensity of the light emission along the column and comparing it with the light emission calibration performed.

The resonant cavity approach is limited in all cases by the fact that above a certain value of electron density and gas pressure, it becomes impossible to obtain a sufficiently well-defined resonance peak because it is too damped/distorted. In addition, for large diameter discharge tubes, the resonant cavity (whose diameter must be much larger than the discharge tube orifice for it to work properly) becomes cumbersome and heavy. The resonant cavity method was used in figures 2, 5, 6 and 8.

Electron density measurement with the TM_{010} resonant cavity [39] was also used to establish the phase diagram of the travelling wave that maintains the discharge, namely ω/ω_{pe} (ω is constant) vs. βR where wave number $\beta = 2\pi/\lambda$, λ being the TW wavelength detected as a function of axial position with an E antenna²¹ moving along the discharge tube: this feeds a first branch of a double balance mixer²², the second branch being connected to the RF generator as a phase reference. The resulting phase variation is shown in figure A1 on the left, insert c [56].

Figure A1 on the right shows the data points ω/ω_{pe} as a function of βR , compared with the phase diagram calculated assuming a cold plasma of locally uniform electron density and a surface-wave discharge. The agreement between experiment and theory is (surprisingly) good, noting however that the calculated curved *overshoot*, attributed to the permittivity of the dielectric tube, should not appear in this diagram since it is irrelevant in our model of TW propagation. In fact, the minimum observed electron density (maximum ω/ω_{pe} value) in the phase diagram is related to the factor $(1 + \varepsilon_g)$, which appears in relation (2).

²¹ The antenna used to collect the wave's electric field strength consists of a semi-rigid coaxial cable with a few mm of its conductive sheath removed. The antenna is oriented perpendicular to the axis of the tube, about one millimetre from its outer wall.

²² The double balanced mixer, followed by a low-pass frequency filter, acts as a phase detector, converting instantaneous phase fluctuations into voltage fluctuations.

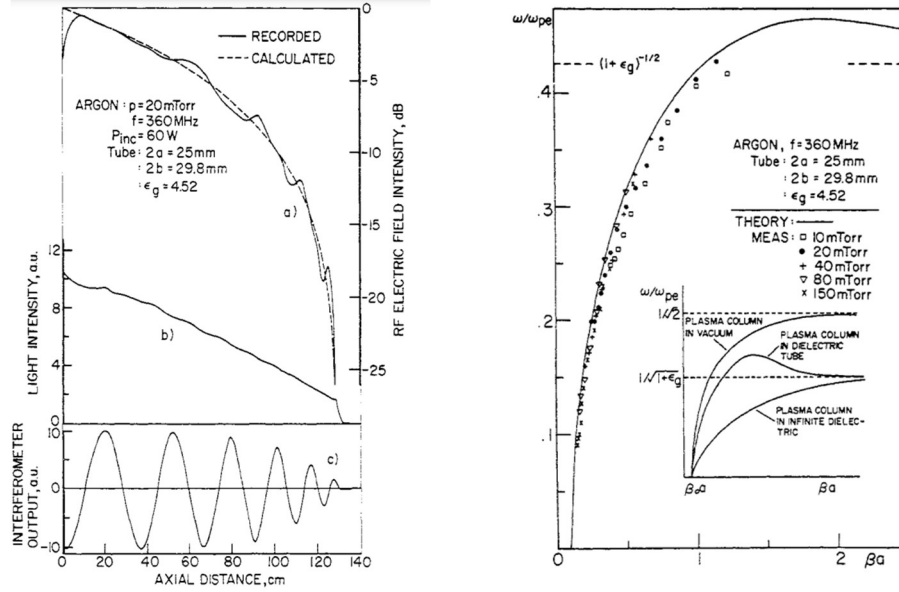


Figure A1. Left: a) RF electric field intensity recorded with an E antenna as a function of axial position along the discharge tube; b) light intensity recorded as a function of axial position on the outside of the discharge tube; c) phase variation of the TW at the output from the balance mixer as a function of axial position [53]. Right: data points of the TW phase diagram compared to the calculated one assuming a surface-wave discharge [53]. The minimum electron density (maximum ω/ω_{pe} ratio), determined along the plasma column with a TM_{010} resonant cavity, is reached following relation (2).

-2 Electron density was also diagnosed from the Stark broadening of the H_{β} emission line (486.1 nm), with hydrogen atoms made available in different ways: i) in an atmospheric pressure neon discharge (figure 7), hydrogen atoms were supplied by a minimal amount of water vapour in the discharge gas, verifying that it did not alter the length of the plasma column [18]; ii) in an atmospheric pressure argon-hydrogen gas mixture containing 0.5% hydrogen, it was also verified that the plasma column with and without added hydrogen retained approximately the same length (figure 4) [14]; iii) in a 9:1 argon/ H_2 gas mixture in a TIAGO torch plasma at atmospheric pressure (figure A4) [40].

-3 Another possible method of diagnosing electron density has been to record the axial phase variation of the TW and use an experimental or calculated TW *phase diagram* (as in figure A1 right) to relate the recorded TW wavelength to electron density [19]. The advantage of this method (figures 1 and 3) is that, as mentioned, it can be used with larger diameter discharge tubes and at higher gas pressures than resonant cavities. There is, nonetheless, an upper pressure limit often reached with atmospheric pressure gas discharges, where accurate electron number density determination becomes limited once the TW phase diagram ceases to vary significantly with β (e.g. [14]).

-4 Figure A2 refers to a surfatron plasma at 2450 MHz and at 20 mbars in a discharge tube of $R = 3$ mm with $\epsilon_g = 3.84$. It shows the axial electron density obtained from Thomson scattering, providing a high spatial and temporal resolution, which can be applied non-intrusively to a surface wave plasma [11]. "This is an active spectroscopic method based on the scattering of laser photons by free electrons in the plasma. It does not need any model to account for the state of equilibrium departure" [11]. Figure A2 shows that the axial distribution of the electron density is linear, provided that the measurement point closest to the surfatron, due to the antenna-like radiation from the field applicator, is not considered. In figure 13a, with the same scheme but at a higher gas pressure, 40 and 80 mbar, the observed axial distribution of electron density is no longer linear

since the TW plasma column then undergoes radial contraction and only part of the radial electron density is taken into account due to the very narrow width of the probing laser beam.

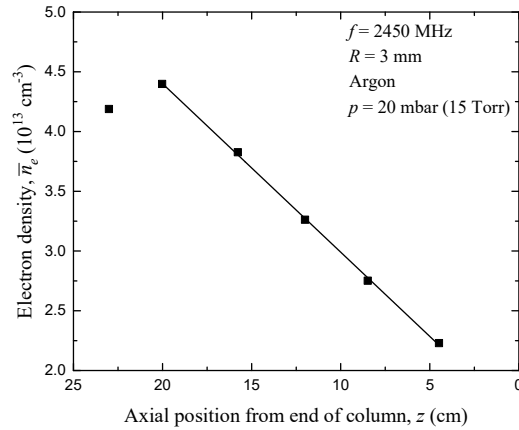


Figure A2 (foreign laboratory). Axial distribution of electron density measured by Thomson scattering along a surfatron plasma operated at 2450 MHz in a $R = 3$ mm tube and at 20 mbars (15 Torr) [11]. Beyond the data point closest to the field-applicator (antenna-like radiation), the plasma column is linear and ends abruptly without transition.

5- Figure A3 shows the electron density (\bar{n}_e) along a surfatron plasma at 2450 MHz and at 15 mbar (11.2 Torr) in a $R = 3$ mm tube with $\epsilon_g = 3.84$, obtained from the continuum radiation of the 648 nm line calibrated with a standard tungsten ribbon lamp and expressed in absolute units [41]. The axial distribution of the electron density is again fully linear if we ignore the data point closest to the surfatron, resulting from the antenna-like radiation of the field applicator.

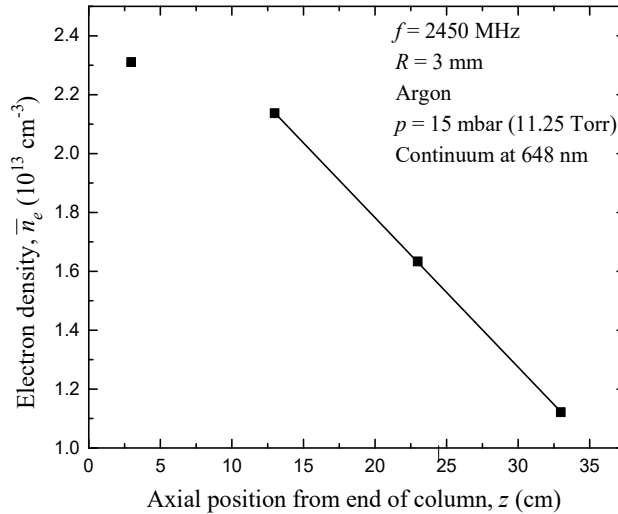


Figure A3 (foreign laboratory). Axial distribution of electron density measured through the continuum radiation from the 648 nm argon line calibrated with a standard tungsten ribbon lamp and expressed in absolute units [41].

6- The ion saturation current from a Langmuir probe matched with a reference probe placed inside the surfatron was used to determine the axial distribution of electron density [22] in figures 11

and 12. Figure 11 showed electron density values below the minimum electron density $\bar{n}_{e(re)}$ for TW propagation, which is incorrect probably due to an underestimation of the ion saturation current.

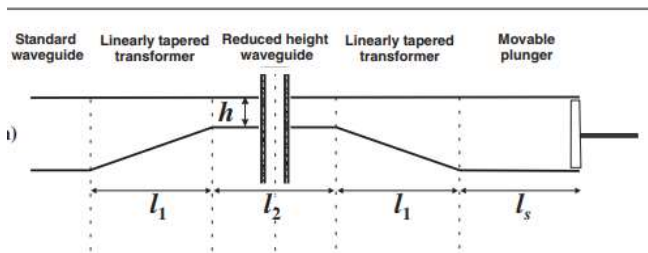
Irrespective of the electron density measurement technique used and disregarding the contribution of the antenna-like EM radiation region of the field applicator, the different measurement methods lead to an axial electron density distribution that decreases linearly and stops without transition at the end of the plasma column. To observe such linear behaviour in the event of radial contraction of the plasma column, the complete radial distribution of electrons at each axial position must be taken into account.

Appendix B: the TIA/TIAGO "surface-wave" sustained plasma torch

Figure A4a shows a schematic cross-sectional representation of the TIA/TIAGO microwave field-applicator: a hollow conductive rod, terminated by a conical nozzle, emerges from a so-called surfaguide field-applicator [42]²³ through the broad front (thinned) and rear walls of a section of reduced-height following the narrow walls of a standard rectangular waveguide so modified. The pre-mixed He/H₂ 9/1 gas flows at a velocity of 10 slm through the inner duct of the rod to exit at the end of the nozzle through a 1 mm diameter orifice. The discharge is maintained at 2450 MHz with 700 W [43]. The *plasma flame*, as illustrated in figure A4a, consists of the *dart* embedded in the *plume*, which extends further out.

Figure A4b shows the radial mean electron density obtained from the Stark broadening of the H_{β} line along the filamentary plasma relative to the nozzle tip [43,44]. Excluding the first two axial data points belonging to the antenna-like radiation region [7] and the last two assumed to be affected by ambient N_2 penetrating the plasma filament, the least-squares regression ($r^2 = 0.999$) reveals a truly linearly decreasing axial distribution of electron density from a distance of 3.5 mm from the nozzle tip. Details on the dart and plasma flame composition can be found in [45].

¹⁹ The surfaguide is typically fabricated from a standard WR-340 (R26) rectangular waveguide and consists of three distinct parts: a central reduced-height section h of the narrow waveguide wall and of length l_2 , and two linearly reduced sections, each of length l_1 , providing a continuous and gradual transition from the central section to the two ends of the standard waveguide, namely the power input side and the moving shorting plane of length l_s [42]. Two circular holes are drilled through the centre of the reduced-height section of the surfaguide through its broad walls, forming a launching gap from which a travelling wave is excited, in this case, along the conductive rod. The height h of the waveguide tapering should not be chosen as narrow as possible having in mind to enhance the E -field intensity in the launching interstice, but at the height that ensures that the characteristic impedance of the TWD, seen as a transmission line, matches that of the surfaguide at its launching aperture [1].



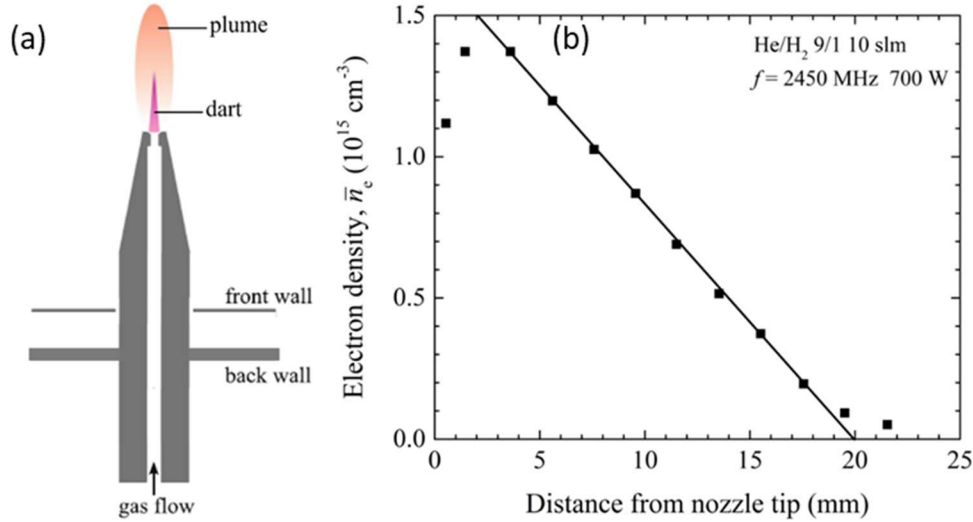


Figure A4. a) shows a schematic diagram of the TIAGO MW plasma torch. It consists of a hollow conducting rod through which the carrier gas flows towards the nozzle, with an outlet hole of 1 mm in diameter [12, 14, 15]. This plasma is supported by a travelling EM wave launched from the *gap* in the surfaguide, a space of reduced height, delimited by the broad front and rear walls. The TW gives rise to a dense plasma filament, the *dart*, and a diffuse plasma surrounding it, the *plume*; b) the plasma is generated in a premixed He/H₂ 9/1 gas flowing at a speed of 10 standard litres per minute (slm) and sustained at 2450 MHz with a power of 700 W [12]. The figure shows the average electron density obtained from the Stark broadening of the H β line along the filamentary plasma [18, 19].

The fact that the electron density distribution decreases linearly along the plasma filament maintained by a TW reminds us that the discharge is controlled by the Zakrzewski stability criterion. Furthermore, the travelling wave that heats the electrons in the discharge gas can only do so by propagating outside the plasma filament in the ambient carrier gas (vacuum).

A proven application of the TIAGO among others is the abundant (and efficient) production of graphene [46]. The efficiency of the TIAGO torch could probably be higher when reducing the diameter of the exiting orifice, which amounts to decreasing the volume of the plasma produced while keeping the MW field area the same [9]. A high MW power ($> 10 \text{ kW}$) variant of this device has also been patented [47].

Appendix C: various electron density distributions along plasma columns supported by the E field of the standing wave arising from the interference of two travelling waves

The obtaining of a standing wave by the interference of two guided travelling waves supporting the plasma column prevents the perfect linear decrease of the axial distribution of electron density associated with a travelling wave, reducing the extent of axial variation of electron density. The standing wave configurations to be discussed arise from the interference of two travelling waves of different azimuthal modes or the same mode.

1- Interference near the end of the plasma column of an azimuthally symmetric ($m = 0$) travelling wave with its equivalent dipolar ($m = 1$) wave.

Figure 15b shows alternating light and dark circular rings along the axis of the plasma column near its tip. These rings are due to the interference of two travelling waves, one of $m = 0$ mode and the other of $m = 1$ mode, which are reflected at the end of the plasma column. For this to be possible, the value of the product fR must be sufficiently high for the wave of the $m = 1$ mode to be excited, but not so high that the $m = 0$ wave no longer exists: the exclusive presence of the $m = 1$ TW mode

[48] starts at $fR = 1.8$ GHz-cm. In figure 15b, the radius of the discharge tube is 1.07 cm and the frequency of the wave that maintains the plasma column is 915 MHz, giving an fR product of 0.98 GHz-cm that effectively allows the coexistence of the $m = 0$ and $m = 1$ TW propagation modes [43].

It is interesting to note at this point that the selection of the TW propagation modes depends on the operating parameters f and R , whose essential role in defining the properties of plasma columns maintained by travelling waves was already demonstrated in section 2.

2- Interference between two independently launched azimuthally symmetric ($m = 0$) travelling waves.

a) Figure A5a shows the experimental arrangement used for this purpose by Rakem et al [49]. The surfaguide field-applicator is accompanied by a discharge tube with a radius that is not too large [48] ensuring to excite a pure TW $m = 0$ mode on each side, in a direction opposite to each other²⁴. The wave initially excited in the direction of the plane of the "short-circuit 1" reflector (at the extreme left of figure A5a) is reflected to pass through the wave-launching aperture of the surfaguide, this back wave then propagating in the same direction as the front travelling wave. These two waves travel together to "short circuit 2" where they are reflected, then interfere (due to their phase difference) with each other on their return path, giving rise to figure A5b for the radial component of the wave E -field along the plasma column and figure A5c for the axial distribution of the electron density.

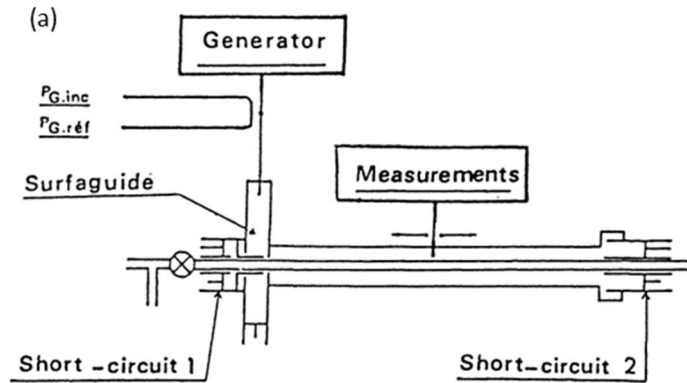


Figure A5a) (foreign laboratory). Experimental arrangement [45]: a surfaguide operating at 2450 MHz with 70 W provides an argon TWD at 0.5 Torr in a fused silica tube with an inner and outer radius 2.5/5 mm. A radially oriented antenna to record the E MW field component of the TWD or an optical collection device, attached to a spectrophotometer, both move on a platform over an axial length of 100 mm along the discharge tube.

²⁴ The surfaguide can generate a TW in both directions from its launching gap along the discharge tube.

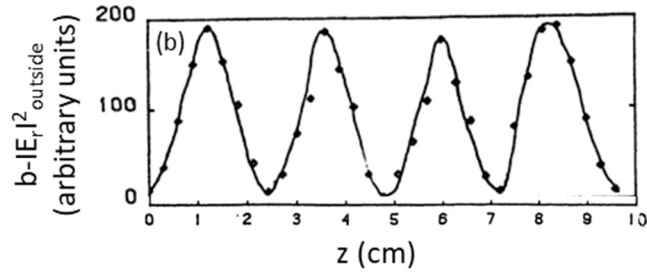


Figure A5b (foreign laboratory). Radial component of the TW E -field in the standing wave mode as observed with a MW electric-field antenna radially oriented and carried by a chain-driven platform along the external wall of the discharge tube [49].

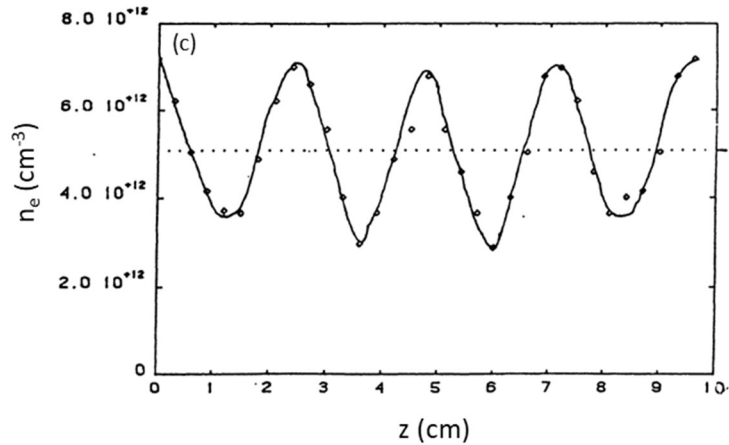


Figure A5c (foreign laboratory). Average radial electron density determined along the discharge tube by the TW phase variation technique [19]. The electron density is modulated around an average value of $5.1 \cdot 10^{12} \text{ cm}^{-3}$ for an absorbed power of only 70 W, whereas it would take around 200 W to obtain the same value of electron density at the start of the plasma column maintained by a travelling wave [49].

b) Another possible standing wave configuration, proposed by Chaker et al. [16], comes from using two launchers, each located at one end of the discharge tube and supplying them from two separate MW generators, which are thus not phase related. This method gives improved axial uniformity over that in paragraph 2a); adjusting the power of each generator correctly for best uniformity can be critical.

c) A 2450 MHz surfguide is placed at each end of the discharge tube, creating a standing wave along the plasma column by the interference of the two $m = 0$ TWs launched independently, but in phase this time (same generator, 3 dB power divider). This original arrangement proposed by Wolinska-Szatkowska [50] for obtaining a standing wave along the plasma column nevertheless gives similar experimental results as in paragraph 2a) above.

d) The following experiment is designed to assess the relative importance (in maintaining the plasma column) of the contribution of the electric field components E_z and E_r of the $m = 0$ azimuthally symmetric travelling wave under conditions where the plasma column is maintained by high intensity standing waves [51]. Particular attention is paid to the determination of the axial distribution of the electron density under more efficient wave reflection conditions. This is again presented as a means of reducing the axial non-uniformity of the plasma column compared with that maintained by a purely travelling wave.

The experimental arrangement shown in diagram A6 can be regarded as an open-air interferometer. It consists of two MW reflecting conductor planes (copper mirrors) M1 and M2, through the centre of which passes the discharge tube positioned perpendicular to the mirrors, the distance between them being adjustable using the M2 mirror. The originality of the assembly lies in the presence of a copper reflector mesh inserted transversely into the discharge tube and of the same internal diameter, to make the surface of the reflective plane of mirror M2 completely uniform (no discontinuities), taking into account the orifice through which the discharge tube passes. This reflector net and the mirror M2 can also be moved independently of each other.

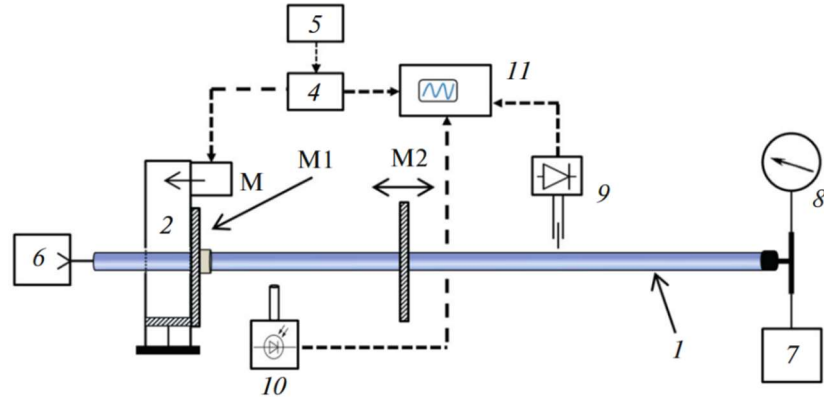


Figure A6 (foreign). Schematic diagram of the experimental set-up: (1) fused silica discharge tube, 2 m long with an inner and outer radius of 5 and 7 mm, (2) waveguide field applicator, (M) magnetron generator at 2450 MHz, (4) square wave modulator with a duration of 50 ms, (5) delayed pulse generator, (6) vacuum pump, (7) gas inlet valve, (8) vacuum gauge, (9) microwave electric field probe, (10) collimated photodetector, (11) oscilloscope, M1, stationary mirror, and M2, axially displaced mirror [51].

The TW plasma column was obtained in argon at 0.25 and 6.5 Torr (~33 and 870 Pa), which, according to the authors, corresponds to $v/\omega \ll 1$. To excite a standing wave with a high VSWR, the distance between the mirrors was chosen to be divisible by an integer number of TW half-wavelengths. This led to a modulation of the plasma density along the column as shown in figure A7, whose maxima and minima coincide with the maxima and minima of the longitudinal component of the E_z field, confirming the dominant role of this component compared with E_r , from which it is offset by 180 degrees.

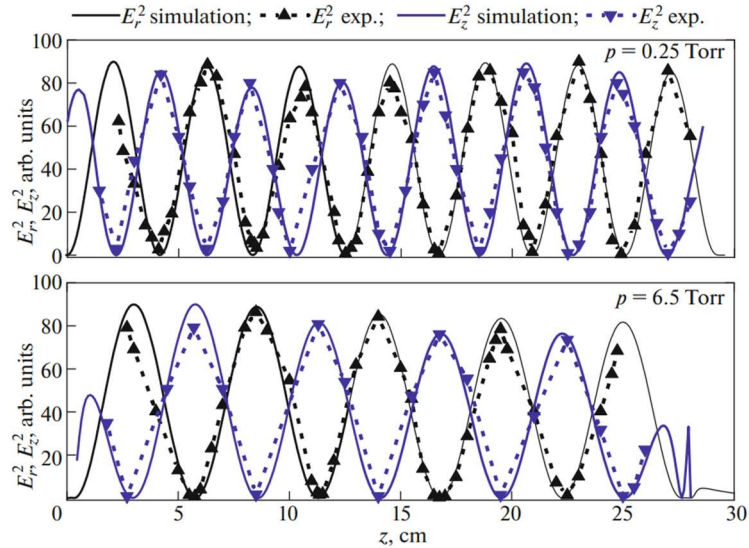


Figure A7 (foreign). Axial distribution of the squared radial and longitudinal components of the TW electric field confined between the two mirrors at pressures of 0.25 and 6.5 Torr. The solid curves are the result of a computer simulation, and the dashed curves are experimental [51].

The use of standing waves, as already mentioned, homogenises the plasma column to some extent compared with the linearly decreasing axial distribution of electron density of a plasma column supported by a travelling wave. Improving the axial uniformity of the TW plasma column properties could be useful in certain applications (e.g. lasers, lighting). The idea of obtaining a plasma column supported by "surface waves" in standing-wave mode was first proposed by Rogers and Asmussen [52].

Acknowledgments

The contribution of Dr. Helena Nowakowska (Institute of Flowing Flow Machinery of the Polish Academy of Sciences, Gdansk, Poland) to a group of equations derived in section 3 is gratefully acknowledged. Professors Émile Carbone (INRS-Énergie, Matériaux, Télécommunications, Varennes, Québec), Vasco Guerra (Instituto Superior Técnico, Lisboa, Portugal) and J.J.A.M. Van der Mullen (Eindhoven University of Technology, The Netherlands and Université Libre de Bruxelles, Belgium) are to be thanked for their comments on the manuscript during its preparation. We are also indebted to Dr. Mariam Rachidi (Montréal, Québec) for data processing. The Natural Sciences and Engineering Research Council of Canada (NSERC) covered the costs of editing and publishing this manuscript.

References

1. Moisan, M.; Nowakowska, H. Contribution of surface-wave (SW) sustained plasma columns to the modeling of RF and microwave discharges. *Plasma Sources Science and Technology* **2018**, *27*, 073001-073044, doi:10.1088/1361-6595/aac528.
2. Zhelyazkov, I.; Atanassov, V. Axial structure of low-pressure high-frequency discharges sustained by travelling electromagnetic surface waves. *Physics Reports* **1995**, *255*, 79-201.
3. Kabouzi, Y.; Moisan, M.; Rostaing, J.C.; Trassy, C.; Guérin, D.; Kéroack, D.; Zakrzewski, Z. Abatement of perfluorinated compounds using microwave plasmas at atmospheric pressure. *Journal of Applied Physics* **2003**, *93*, 9483-9496.
4. Glaude, V.M.M.; Moisan, M.; Pantel, R.; Leprince, P.; Marec, J. Axial electron-density and wave power distributions along a plasma-column sustained by the propagation of a surface microwave. *Journal of Applied Physics* **1980**, *51*, 5693-5698, doi:10.1063/1.327568.
5. Chaker, M.; Moisan, M. Large-diameter plasma columns produced by surface waves at radio and microwave frequencies. *Journal of Applied Physics* **1985**, *57*, 91-95, doi:10.1063/1.335401.
6. Nowakowska, H.; Lackowski, M.; Moisan, M. Radiation losses from a microwave surface-wave (SW) sustained plasma source (surfatron). *IEEE Transactions on Plasma Science* **2020**, *48*, 2106-2114, doi:10.1109/TPS.2020.2995475.
7. Moisan, M.; Levif, P.; Nowakowska, H. Space-wave (antenna) radiation from the wave launcher (surfatron) before the development of the plasma column sustained by the EM surface wave: a source of microwave power loss. *AMPERE Newsletter* **2019**, 9-19.
8. Matejka, J.; Fitzmaurice, G. Same stats, different graphs: generating datasets with varied appearance and identical statistics through simulated annealing. In Proceedings of the 2017 CHI Conference on Human Factors in Computing Systems, 2017; pp. 1290–1294.
9. Aliev, Y.M.; Schlüter, H.; Shivarova, A. *Guided-wave-produced plasmas*; Springer: Berlin, 2000.
10. Moisan, M.; Ganachev, I.P.; Nowakowska, H. Concept of power absorbed and lost per electron in surface-wave plasma columns and its contribution to the advanced understanding and modeling of microwave discharges. *Physical Review E* **2022**, *106*, 045202.
11. Palomares, J.M.; Iordanova, E.; van Veldhuizen, E.M.; Baede, L.; Gamero, A.; Sola, A.; van der Mullen, J.J.A.M. Thomson scattering on argon surfatron plasmas at intermediate pressures: Axial profiles of the electron temperature and electron density. *Spectrochimica Acta Part B: Atomic Spectroscopy* **2010**, *65*, 225-233.
12. Moisan, M.; Zakrzewski, Z. Plasma sources based on the propagation of electromagnetic surface waves. *Journal of Physics D: Applied Physics* **1991**, *25*, 1025-1048.
13. Sola, A.; Cotrino, J.; Colomer, J. Reexamination of recent experimental results in surface-wave-produced argon plasmas at 2.45 GHz: Comparison with the diffusion-recombination model results. *Journal of Applied Physics* **1988**, *64*, 3419-3423.
14. Moisan, M.; Pantel, R.; Hubert, J. Propagation of surface wave sustaining a plasma column at atmospheric pressure. *Contributions to Plasma Physics* **1990**, *30*, 293-314, doi:10.1002/Ctpp.2150300213.
15. Kovačević, M.S.; Kuzmanović, L.; Milošević, M.M.; Djordjevich, A. An estimation of the axial structure of surface-wave produced plasma column. *Physics of Plasmas* **2021**, *28*, 023502.

16. Chaker, M.; Moisan, M.; Zakrzewski, Z. Microwave and RF surface-wave sustained discharges as plasma sources for plasma chemistry and plasma processing. *Plasma Chemistry and Plasma Processing* **1986**, *6*, 79-96, doi:10.1007/BF00573823.
17. Castaños-Martínez, E.; Moisan, M. Expansion/homogenization of contracted/filamentary microwave discharges at atmospheric pressure. *IEEE Transactions on Plasma Science* **2011**, *39*, 2192-2193.
18. Castaños-Martínez, E. Influence de la fréquence d'excitation sur les phénomènes de contraction et de filamentation dans les décharges micro-ondes entretenues à la pression atmosphérique. Université de Montréal, 2004.
19. Margot-Chaker, J.; Moisan, M.; Zakrzewski, Z.; Glaude, V.M.; Sauvé, G. Phase sensitive methods to determine the wavelength of electromagnetic waves in lossy nonuniform media: The case of surface waves along plasma columns. *Radio Science* **1988**, *23*, 1120-1132, doi:10.1029/RS023i006p01120.
20. Moisan, M.; Pelletier, J. *Physics of collisional plasmas: Introduction to high-frequency discharges*; Springer: Berlin, 2012.
21. Martínez-Aguilar, J.; González-Gago, C.; Castaños-Martínez, E.; Muñoz, J.; Calzada, M.D.; Rincón, R. Influence of gas flow on the axial distribution of densities, temperatures and thermodynamic equilibrium degree in surface-wave plasmas sustained at atmospheric pressure. *Spectrochimica Acta Part B: Atomic Spectroscopy* **2019**, *158*, 1-9.
22. Dias, F.M.; Tatarova, E.; Ferreira, C.M. Spatially resolved experimental investigation of a surface wave sustained discharge in nitrogen. *Journal of Applied Physics* **1998**, *83*, 4602-4609.
23. Gordiets, B.; Pinheiro, M.; Tatarova, E.; Dias, F.M.; Ferreira, C.M.; Ricard, A. A travelling wave sustained hydrogen discharge: modelling and experiment. *Plasma Sources science and Technology* **2000**, *9*, 295-303.
24. Hübner, S. Poly-diagnostic study of low pressure microwave plasmas. Technische Universiteit Eindhoven, Netherlands, 2013.
25. Carbone, E.A.D.; Hubner, S.; Jimenez-Diaz, M.; Palomares, J.M.; Iordanova, E.; Graef, W.A.A.D.; Gamero, A.; van der Mullen, J.J.A.M. Experimental investigation of the electron energy distribution function (EEDF) by Thomson scattering and optical emission spectroscopy. *Journal of Physics D: Applied Physics* **2012**, *45*, 475202.
26. Aliev, Y.M.; Boev, A.G.; Shivarova, A. On the non-linear theory of a long gas discharge produced by an ionizing slow electromagnetic wave. *Physics Letters* **1982**, *92*, 235-237.
27. Zakrzewski, Z. Conditions of existence and axial structure of long microwave discharges sustained by travelling waves. *Journal of Physics D: Applied Physics* **1983**, *16*, 171-180, doi:10.1088/0022-3727/16/2/014.
28. Moisan, M.; Barbeau, C.; Claude, R.; Ferreira; Margot, J.; Paraszczak, J.; Sá, A.B.; Sauvé, G.; Wertheimer, M.R. Radio-frequency or microwave plasma reactors - factors determining the optimum frequency of operation. *Journal of Vacuum Science and Technology B* **1991**, *9*, 8-25, doi:10.1116/1.585795.
29. Hamdan, A.; Valade, F.; Margot, J.; Vidal, F.; Matte, J.P. Space and time structure of helium pulsed surface-wave discharges at intermediate pressures (5–50 Torr). *Plasma Sources Science and Technology* **2017**, *26*, 015001, doi:10.1088/0963-0252/26/1/015001.
30. Aliev, Y.M.; Boev, A.G.; Shivarova, A. Slow ionizing high-frequency electromagnetic wave along a thin plasma column. *Journal of Physics D: Applied Physics* **1984**, *17*, 2233-2242.
31. Mateev, E.; Zhelyazkov, I.; Atanassov, V. Propagation of a large amplitude surface wave in a plasma column sustained by the wave. *Journal of Applied Physics* **1983**, *54*, 3049-3052.

32. Zhelyazkov, I.; Benova, E.; Atanassov, V. Axial structure of a plasma column produced by a large-amplitude electromagnetic surface wave. *Journal of Applied Physics* **1986**, *59*, 1466-1472.
33. Aliev, Y.M.; Maximov, A.V.; Schluter, H.; Shivarova, A. On the axial structure of surface wave sustained discharges. *Physica Scripta* **1995**, *51*, 257-262.
34. Aliev, Y.M.; Ivanova, K.M.; Moisan, M.; Shivarova, A. Analytical expression for the axial structure of surface wave sustained plasmas under various regimes of charged particle loss. *Plasma Sources Science and Technology* **1993**, *2*, 145-152.
35. Babović, V.M.; Aničin, B.A.; Davidović, D.M. The square root approximation to the dispersion relation of the axially-symmetric electron wave on a cylindrical plasma, *Z. Naturforsch* **1997**, *52a*, 709.
36. Hubert, J.; Moisan, M.; Zakrzewski, Z. On the supply and measurement of power in microwave induced plasmas. *Spectrochimica Acta* **1986**, *41B*, 205-215.
37. Czyłkowski, D.; Nowakowska, H.; Mizeraczyk, J.; Zakrzewski, Z. Influence of discharge tube wall thickness on surface-wave discharge parameters. In Proceedings of the 28th ICPIG, Prague, Czech Republic, 2007.
38. Aliev, Y.M.; Maximov, A.V.; Ghanashev, I.; Shivarova, A.; Schlüter, H. Axial structure of discharges sustained by ionizing fast electromagnetic surface waves. *IEEE Transactions on Plasma Science* **1995**, *23*, 409-414.
39. Zakrewski, Z.; Moisan, M.; Leprince, P. Attenuation of a surface-wave in an unmagnetized RF plasma column. *Plasma Physics and Controlled Fusion* **1977**, *19*, 77-83.
40. Castañós-Martínez, E.; Kabouzi, Y.; Makasheva, K.; Moisan, M. Modeling of microwave-sustained plasmas at atmospheric pressure with application to discharge contraction. *Physical Review E* **2004**, *70*, 066405.
41. Iordanova, E.; de Vries, N.; Guillemier, M.; van der Mullen, J.J.A.M. Absolute measurements of the continuum radiation to determine the electron density in a microwave-induced argon plasma. *Journal of Physics D: Applied Physics* **2008**, *41*, 015208.
42. Fleisch, T.; Kabouzi, Y.; Moisan, M.; Pollak, J.; Castañós-Martínez, E.; Nowakowska, H.; Zakrzewski, Z. Designing an efficient microwave-plasma source, independent of operating conditions, at atmospheric pressure. *Plasma Sources Science and Technology* **2007**, *16*, 173–182, doi:10.1088/0963-0252/16/1/022.
43. Ricard, A.; St-Onge, L.; Malvos, H.; Gicquel, A.; Hubert, J.; Moisan, M. Torche à plasma à excitation micro-onde : deux configurations complémentaires. *Journal de Physique III France* **1995**, *5*, 1269-1285.
44. Moisan, M.; Kéroack, D.; Stafford, L. *Physique atomique et spectroscopie optique. Collection Grenoble Sciences (EDP)*; Les Ulis: France, 2016.
45. Morales-Calero, F.J.; Rincón, R.; Muñoz, J.; Calzada, M.D. Experimental characterization of TIAGO torch discharges: surface wave discharge behavior and (post-)discharge kinetics. *Plasma Sources Science and Technology* **2023**, *32*, 065001, doi:10.1088/1361-6595/acd3a8.
46. Melero, C.; Rincón, R.; Muñoz, J.; Zhang, G.; Sun, S.; Perez, A.; Royuela, O.; González-Gago, C.; Calzada, M.D. Scalable graphene production from ethanol decomposition by microwave argon plasma torch. *Plasma Physics and Controlled Fusion* **2018**, *60*, 014009, doi:10.1088/1361-6587/aa8480.
47. Larquet, C.; Guérin, D.; Rostaing, J.-C.; Dulphy, H.; Moisan, M. Procédé et dispositif de traitement effluents gazeux de procédés industriel. 2006, France, Air Liquide.
48. Margot-Chaker, J.; Moisan, M.; Chaker, M.; Glaude, V.M.M.; Lauque, P.; Paraszczak, J.; Sauvé, G. Tube diameter and wave frequency limitations when using the electromagnetic

- surface wave in the $m=1$ (dipolar) mode to sustain a plasma column. *Journal of Applied Physics* **1989**, *66*, 4134-4148, doi:10.1063/1.343998.
49. Rakem, Z.; Leprince, P.; Marec, J. Characteristics of a surface wave produced discharge operating under standing wave conditions. *Revue de Physique Appliquée* **1990**, *25*, 125-130.
 50. Wolinska-Szatkowska, J. The modelling of a discharge sustained by a standing surface wave. *Journal of Physics D: Applied Physics* **1988**, *21*, 937-943.
 51. Zhukov, V.I.; Karfidov, D.M. Plasma distribution in a column of a low-pressure microwave discharge sustained by a standing surface wave. *Plasma Physics Reports* **2023**, *49*, 975-983, doi:10.1134/S1063780X23600792.
 52. Rogers, J.; Asmussen, J. Standing waves along a microwave generated surface wave plasma. *IEEE Transactions on Plasma Science* **1982**, *10*, 11-16.
 53. Zakrzewski, Z.; Moisan, M.; Glaude, V. M. M.; Beaudry, G.; Leprince, P. Attenuation of a surface wave in an unmagnetized R. F. plasma column. *Plasma Physics* **1977**, *19*, 77-83.